Circulation

ORIGINAL RESEARCH ARTICLE

Small Extracellular Vesicles From Infarcted and Failing Heart Accelerate Tumor Growth

Tal Caller, MSc; Itai Rotem, PhD; Olga Shaihov-Teper, MSc; Daria Lendengolts, DVM; Yeshai Schary, MSc; Ruty Shai, PhD; Efrat Glick-Saar, PhD; Dan Dominissini, PhD; Menachem Motiei, PhD; Idan Katzir, MSc; Rachela Popovtzer, PhD; Merav Nahmoud; Alex Boomgarden, MSc; Crislyn D'Souza-Schorey, PhD; Nili Naftali-Shani, PhD; Jonathan Leor, MD

BACKGROUND: Myocardial infarction (MI) and heart failure are associated with an increased incidence of cancer. However, the mechanism is complex and unclear. Here, we aimed to test our hypothesis that cardiac small extracellular vesicles (sEVs), particularly cardiac mesenchymal stromal cell–derived sEVs (cMSC-sEVs), contribute to the link between post-MI left ventricular dysfunction (LVD) and cancer.

METHODS: We purified and characterized sEVs from post-MI hearts and cultured cMSCs. Then, we analyzed cMSC-EV cargo and proneoplastic effects on several lines of cancer cells, macrophages, and endothelial cells. Next, we modeled heterotopic and orthotopic lung and breast cancer tumors in mice with post-MI LVD. We transferred cMSC-sEVs to assess sEV biodistribution and its effect on tumor growth. Finally, we tested the effects of sEV depletion and spironolactone treatment on cMSC-EV release and tumor growth.

RESULTS: Post-MI hearts, particularly cMSCs, produced more sEVs with proneoplastic cargo than nonfailing hearts did. Proteomic analysis revealed unique protein profiles and higher quantities of tumor-promoting cytokines, proteins, and microRNAs in cMSC-sEVs from post-MI hearts. The proneoplastic effects of cMSC-sEVs varied with different types of cancer, with lung and colon cancers being more affected than melanoma and breast cancer cell lines. Post-MI cMSC-sEVs also activated resting macrophages into proangiogenic and protumorigenic states in vitro. At 28-day follow-up, mice with post-MI LVD developed larger heterotopic and orthotopic lung tumors than did sham-MI mice. Adoptive transfer of cMSC-sEVs from post-MI hearts accelerated the growth of heterotopic and orthotopic lung tumors, and biodistribution analysis revealed accumulating cMSC-sEVs in tumor cells along with accelerated tumor cell proliferation. sEV depletion reduced the tumor-promoting effects of MI, and adoptive transfer of cMSC-sEVs from post-MI hearts partially restored these effects. Finally, spironolactone treatment reduced the number of cMSC-sEVs and suppressed tumor growth during post-MI LVD.

CONCLUSIONS: Cardiac sEVs, specifically cMSC-sEVs from post-MI hearts, carry multiple protumorigenic factors. Uptake of cMSC-sEVs by cancer cells accelerates tumor growth. Treatment with spironolactone significantly reduces accelerated tumor growth after MI. Our results provide new insight into the mechanism connecting post-MI LVD to cancer and propose a translational option to mitigate this deadly association.

Key Words: cardio-oncology ■ extracellular vesicles ■ fibroblasts ■ heart failure ■ inflammation ■ mesenchymal stem cells ■ myocardial infarction ■ neoplasms ■ spironolactone

Editorial, see p XXX

Clinical Perspective

What Is New?

- Post–myocardial infarction hearts secrete small extracellular vesicles with proneoplastic properties.
- Cardiac mesenchymal stromal cells are a rich source of extracellular vesicles that accelerate tumor growth.
- Administration of spironolactone reduces the number of cardiac extracellular vesicles and tumor growth in mice with post–myocardial infarction left ventricular dysfunction.

What Are the Clinical Implications?

- Cardiac extracellular vesicles may be used for risk stratification and identifying therapeutic targets in patients with heart disease and cancer.
- Spironolactone mitigates the harmful interaction between post–myocardial infarction left ventricular dysfunction and cancer.
- Our results may apply to the association between other cardiovascular diseases and cancer.

Nonstandard Abbreviations and Acronyms

cEV	cardiac extracellular vesicle
cMSC	cardiac mesenchymal stromal cell
cMSC-sEVs	cardiac mesenchymal stromal cells small extracellular vesicles
COL1α	collagen 1 alpha
EC	endothelial cell
EV	extracellular vesicle
HF	heart failure
IL	interleukin
LLC	Lewis lung carcinoma
LV	left ventricle
LVD	left ventricular dysfunction
MI	myocardial infarction
NT-proBNP	N-terminal pro-brain natriuretic peptide
miR	microRNA
sEVs	small extracellular vesicles
TAM	tumor-associated macrophage
TGFβ	transforming growth factor β
TNFα	tumor necrosis factor α
TSG101	tumor susceptibility gene 101
VEGF	vascular endothelial growth factor

Cancer and heart failure (HF) are common diseases with shared risk factors, mechanistic similarities, and lethal interactions.[1–4] Although anticancer therapies accelerate HF, the presence of HF may increase cancer incidence.[1,5–7] The coexistence of these diseases worsens patients' prognoses and negatively affects therapeutic options.[5,7,8]

The association between HF and cancer is complex and not entirely clear. It is attributed in part to shared risk factors.[1,2] However, recent studies have suggested a more causal explanation: circulating factors released from injured hearts accelerate tumor growth, independent of risk factors.[9–13] However, the link between HF and cancer is not fully understood.[1,2]

A potential unexplored mechanism that may link heart disease to cancer is small extracellular vesicles (sEVs). sEVs (<200 nm) have emerged as a new and powerful mechanism of communication between cells and their environment through the ability of sEVs to transmit multimolecular biological messages with much greater complexity than a single factor.[14–17] sEVs exert their function by altering recipient cells through the delivery of RNA, cytokines, chemokines, growth factors, or surface protein signaling.[14–17] sEVs play a role in disease processes like heart disease and cancer.[15,16] sEVs may mediate the communication between the heart and other organs.[18] However, whether and how sEVs from the failing heart promote tumor growth remains unknown.

Given the central role of sEVs in cell-to-cell communication, we hypothesized that cardiac sEVs contribute to the association between post-MI HF and tumor growth. Here, we tested our hypothesis in a mouse model of post-MI left ventricular dysfunction (LVD) and cancer. Understanding how post-MI LVD may promote cancer could help develop treatments simultaneously targeting both diseases. In addition, understanding the mechanism linking LVD to cancer could help identify patients with cardiovascular disease at higher risk of cancer. It may allow for early risk stratification, prevention, and treatment.

METHODS

Detailed methods are provided in the Supplemental Material. All data that support our findings are available within the article, the Supplemental Material, and on reasonable request. Animal experiments were conducted according to the National Institutes of Health Guide for the Care and Use of Laboratory Animals and complied with the standards and approval of the Sheba Medical Center institutional animal care and use committee.

We purified and characterized sEVs from the whole heart or isolated cardiac mesenchymal stromal cells (cMSCs). We analyzed cMSC-sEV size distribution, markers, cargo, and effects on cancer cells, endothelial cells (ECs), macrophage activation, and tumor growth. We modeled post-MI LVD in mice, along with heterotopic and orthotopic lung and breast cancer tumors. To monitor LVD, we used a small-animal echocardiography system. To assess tumor growth, we used ultrasound, bioluminescent IVIS Spectrum imaging, and microcomputed tomography. We also used cMSC-extracellular vesicle (EV) transfer to assess sEV biodistribution, uptake, and effects on tumor growth. Finally, we tested the effects of EV depletion and spironolactone treatment on cMSC-EV release and tumor growth.

Statistical Analysis

Data are expressed as mean±SD. Specific statistical tests are detailed in the figure legends. Statistical analyses were performed with GraphPad Prism v9.5.0 unless otherwise stated. Statistical analyses of the identification and quantification of the proteomic analysis (proteomics) were performed using Perseus 1.6.7.0, and statistical analysis for nanoparticle tracking analysis data was performed using STATA BE v17.

A 2-tailed Student t test was used to compare normally distributed continuous variables, and a 2-tailed Mann-Whitney U test was used for nonnormal distribution. When t tests were performed multiple times, multiple testing correction was performed. For experiments with >2 groups, a comparison was performed with 1- or 2-way ANOVA with the Holm-Šídák post test. To test the hypothesis that changes in measures (eg, tumor volumes) over time varied among the experimental groups, a general linear model repeated-measures 2-way ANOVA was used. The Holm-Šídák post hoc test assessed the significance of predefined group comparisons at specific time points. We also used repeated-measures 2-way ANOVA to assess changes in cell migration, left ventricle (LV) remodeling, and function over time. To compare 2-frequency distribution, we used zero-inflated negative binomial regression.

RESULTS

Post-MI LVD Accelerated Heterotopic Tumor Growth

Lung cancer is a frequent and leading cause of death in patients with LVD.[6–8,19] To generate a mouse model of post-MI LVD and cancer and to reproduce previous reports,[10,11] we created a mouse model of heterotopic lung cancer (Figure S1A). First, we inoculated Lewis lung cancer (LLC) cells in the dorsal aspect of a limb of a female C57BL/6 mouse. Then, 10 days later, we randomly assigned mice bearing LLC tumors to MI or sham-MI (Figure S1A). The MI mortality rate was 11% (1 of 9) or null after sham-MI. We confirmed post-MI LVD by echocardiography (Figure 1A; Figure S1B), plasma NT-proBNP (N-terminal pro-brain natriuretic peptide; Figure 1A), and lung congestion (Figure S1C) 10 days after MI. In line with previous reports,[10,11] we found that post-MI LVD accelerated tumor growth and weight (Figure S1D and S1E).

The Infarcted and Failing Heart Generated sEVs With Proneoplastic Properties

To determine the role of cardiac sEVs in tumor growth, we first assessed production of sEVs in the entire myocardium 10 days after MI (Figure S2A). We subjected female C57BL/6 mice to MI or sham-MI. Post-MI LVD in MI mice was confirmed by echocardiography, plasma NT-proBNP (Figure 1A), and lung congestion (Figure S2A). Our method of isolating and purifying whole-heart EVs was inspired by the work of Loyer et al,[20] and we purified sEVs by size exclusion chromatography (Figure S2B).[21,22] To characterize sEVs, we used transmission electron microscopy (Figure S2C) and Western blot for the sEV markers: CD81 and TSG101 (tumor susceptibility gene 101; Figure S2D). Next, we used nanoparticle tracking analysis to determine the morphology and size distribution of sEVs (Figure S2E and S2F). We found that post-MI hearts generated >2-fold the number of sEVs than sham-MI hearts (Figure S2F). Overall, we found that in the early phase of post-MI LVD, the myocardium produced more sEVs.

Next, we assessed the proneoplastic properties of sEVs from post-MI LVD. Compared with sham MI, cEVs from post-MI LVD heart accelerated the proliferation of LLC cells (Figure S2G). The proliferative effects of cEVs followed a dose-response pattern (Figure S1H). Moreover, sEVs from post-MI LVD heart accelerated the migration of LLC cells compared with sham-MI sEVs (Figure S1I), again, with a dose-response pattern (Figure S2J). Post-MI hearts collectively generated a high number of sEVs with proneoplastic properties. However, our experiment neither differentiated between cellular and extracellular vesicles nor identified the cell source of sEVs.

Mesenchymal Stromal Cells from Post-MI Failing Heart Are a Rich Source of sEVs

The heart contains many types and subtypes of cells[23,24]; all are potential sources of sEVs. We focused on cMSCs,[25] because MSCs are activated during tissue injury, repair, and cancer. MSCs have pleiotropic effects, including proinflammatory,[26,27] fibrotic,[28] and tumor-promoting functions.[27,29] Activated cMSCs, particularly fibroblasts, maintain their in vivo signature through at least 4 passages and are therefore suitable for in vitro studies.[30]

First, we isolated and cultured cMSCs 10 days after MI or sham-MI, after resolution of the acute inflammatory phase (Figure 1B).[30] Flow cytometry showed that cMSCs expressed the fibroblast markers COL1α (collagen 1α [94%], CD90 [76%], and mEF-SK4 [98%]; Figure S3A through S3C).[31] The resident fibroblast marker, PDGFRα (platelet-derived growth factor receptor α),[31] was downregulated after MI compared with sham-MI (36% versus 48%; P=0.02; Figure S3D). cMSCs did not express markers of macrophages or ECs (Figure S3E and S3F). Next, after 72 hours of incubation, we collected the serum-free conditioned medium. The viability of cMSCs at the time of medium collection was 90.5% and 86.7% for post-MI and sham-MI cMSCs (Figure S3G). Then, we used size exclusion chromatography to isolate and purify sEVs from the cMSC-conditioned medium (Figure 1B and 1C).[21]

Purified cMSC-sEVs showed typical EV morphology with a double-layer membrane and normal appearance in cryogenic or negative staining transmission electron microscopy (Figure 1D). Western blot confirmed sEV membranous markers CD81 and CD9 and cytosolic markers TSG101 and HSP70 (Figure 1E). Like the
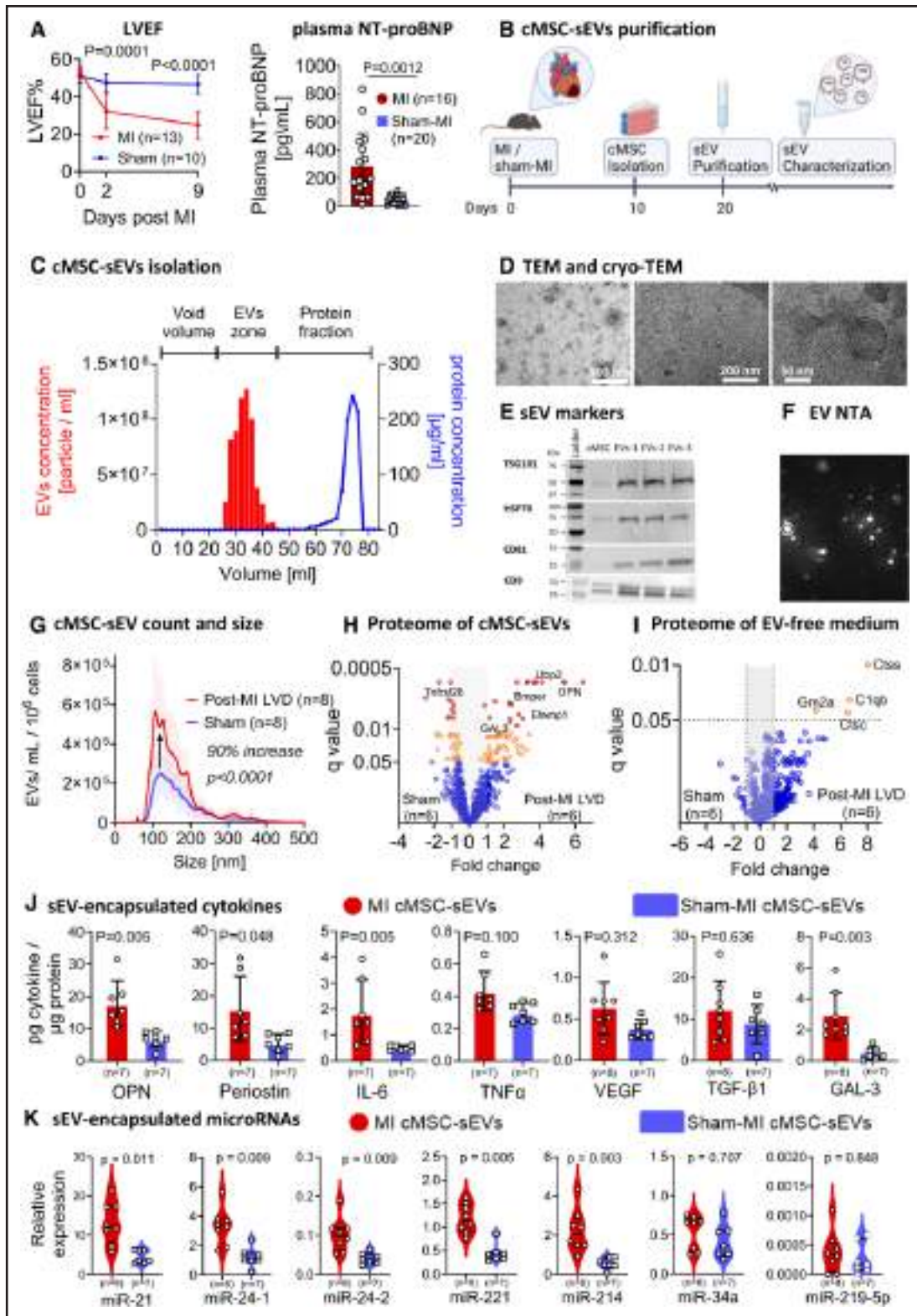
Figure 1. cMSC-sEVs from post-MI failing hearts harbored tumor-promoting factors.
A, MI-induced LVD resulting in elevated plasma NT-proBNP. To monitor cardiac function after MI or sham-MI, we performed serial echocardiography measurements. We calculated LVEF at baseline, day 2, and day 9 after MI. Data are expressed as mean±SD. *P* values were calculated using repeated-measures 2-way ANOVA with the Holm-Šídák post test. *P* for MI, *P* for time, and *P* for interaction were all <0.0001. *P* values for comparisons for MI vs sham-MI are displayed on the graph. Next, we used ELISA to measure plasma NT-proBNP of mice 10 days after MI or sham-MI. The data passed the normality test by D'Agostino-Pearson, and the *P* value was calculated using a 2-tailed unpaired *t* test with Welsch correction for unequal variance. **B**, To isolate cMSC-sEVs, female C57BL/6 mice were randomly assigned to either MI or (*Continued*)

Figure 1 Continued. sham-MI operation. At day 10, hearts were harvested, and cMSCs were isolated by enzymatic digestion and cultured in vitro. At 85% confluence, the medium was replaced by a serum-free medium for 72 hours. Then, EVs were purified from the conditioned medium using size exclusion chromatography. **C,** Size exclusion chromatography successfully separated cMSC-sEVs from soluble proteins. **D,** Typical sEV morphology confirmed by negative staining TEM (**left**) and cryo-TEM (**middle** and **right**). Scale bars from left to right=500 nm, 100 nm, and 50 nm. **E,** The expression of typical EV markers CD81, CD9, TSG101, and HSP70 were determined by a Western blot. **F** and **G,** To assess cMSC-sEV secretion, we used nanoparticle tracking analysis. The post-MI hearts secreted twice as many sEVs as sham-operated hearts. P values were calculated using zero-inflated negative binomial regression, and percent change (MI/sham-MI) was calculated using the ratios of the area under the curves. **H** and **I,** To determine the differences in protein expression between cMSC-sEVs from post-MI and sham-MI hearts, we performed a comparative proteomic analysis. The volcano plot showed a statistically significant change in 114 proteins and a unique profile of cMSC-sEVs from post-MI hearts (**H**). Analysis of EV-free conditioned medium from cMSCs (**I**) revealed modest changes in protein profile compared with the changes observed in cMSC-sEVs. EV-free conditioned medium from cMSCs from the post-MI heart differentially ($q<0.05$) expressed 4 proteins compared with sham-MI. P values were determined by using a t test multiple times with multiple testing corrections (false discovery rate correction). **J,** To investigate cMSC-sEV−encapsulated cytokines, we used ELISA assays. Data are expressed as mean±SD. P values were determined by multiple, 2-tailed, unpaired Mann-Whitney U test with the Holm-Šídák post test to account for multiple comparisons. **K,** To identify miRs within cMSC-sEVs that could influence tumor progression, we used reverse transcription polymerase chain reaction. Compared with sham-MI, we found that cMSC-sEVs from the post-MI heart encapsulated more tumor-promoting miRs, such as miR-21, which promotes digestive system cancers by supporting cell survival, proliferation, migration, and immunomodulation. Other miRs, more abundant in cMSC-sEVs from the post-MI hearts, include miR-24-1, which is associated with ovarian cancer cell proliferation, and miR-24-2, which acts as a tumor suppressor or oncogenic miR, depending on the cancer type, and promotes breast cancer by inducing cell proliferation and lung cancer by supporting angiogenesis. cMSC-sEVs from post-MI hearts also harbored more miR-221, which stimulates tumor development, cancer cell proliferation, and migration, and miR-214, which is upregulated in the lung, breast, prostate, and several other cancer types and may drive tumor development by promoting angiogenesis, cell division, invasion, and metastasis. Other tumor-promoting miRs were detected in similar amounts in cMSCs-EVs from and sham MI: miR-34a, associated with increased cancer cell proliferation and survival, and miR-219-5p, associated with metastasis and growth of gastric and colon cancer, but suppression of ovarian cancer. In addition, miR-208a, associated with tumor cell proliferation and invasion, was undetectable in cMSC-sEVs. Data are expressed as mean±SD. P values were calculated by multiple, 2-tailed, unpaired Mann-Whitney U test with the Holm-Šídák post test to account for multiple comparisons. cMSC indicates cardiac mesenchymal stromal cells; EV, extracellular vesicle; sEVs, small extracellular vesicles; GAL, galectin; IL, interleukin; IFN, interferon; LVD, left ventricular dysfunction; LVEF, left ventricular ejection fraction; MI, myocardial infarction; miR, microRNA; NT-proBNP, N-terminal pro-brain natriuretic peptide; OPN, osteopontin; TEM, transmission electron microscopy; TGF, transforming growth factor; TNF, tumor necrosis factor; and VEGF, vascular endothelial growth factor. Illustration created with BioRender.com.

entire heart, cMSCs from the failing heart secreted twice as many sEVs as cMSCs from sham-MI (Figure 1F and 1G). The size distribution pattern in size exclusion chromatography fractions revealed that most of the sEVs were between 100 and 200 nm (Figure 1G). Overall, we showed that isolating cMSC-sEVs by size exclusion chromatography produces a pure and enriched population of sEVs without contaminated proteins. cMSCs from the failing heart produced more sEVs, mirroring the situation in the whole heart after MI.

Distinct Proteomic Profile of cMSC-sEVs From the Infarcted and Failing Heart

To explore the cargo of cMSC-sEVs, we conducted comparative proteomic profiling and identified 931 cMSC-EV−encapsulated proteins. Comparing cMSC-sEVs from the post-MI heart with those from sham-MI, we found 64 upregulated and 50 downregulated proteins (Figure 1H). For example, osteopontin, a reparative, tumor-promoting protein, was 5.4× higher in cMSC-sEVs from post-MI hearts than from sham-MI hearts. In addition, 174 proteins were detected exclusively in cMSC-sEVs from post-MI hearts, and 31 were absent from cMSC-sEVs from post-MI hearts (Figure S4A). Thus, cMSC-sEVs from the post-MI LVD heart presented a distinct proteomic profile.

To further characterize the proteins from cMSC-sEVs, we analyzed biological pathways using the functional enrichment tool (FunRich) of VesiclePedia using the gene ontology biological processes database.[32] We found that cMSC-sEVs from the failing heart were enriched in pathways related to the development and progression of cancer (Figure S4B).[33] Pathways such as vascular endothelial cell proliferation and mitotic cell cycle phase transition were enriched exclusively in post-MI cMSC-sEVs. Overall, post-MI LVD altered the proteomic profile of cMSC-sEVs toward a reparative and tumor-promoting repertoire.

Analysis of EV-free conditioned medium from cMSCs revealed modest differences in protein profile between cMSCs from failing versus sham-MI hearts (Figure 1I). Thus, our results suggest that the protein cargo of cMSC-sEVs better reflects the environment of the post-MI heart compared with the cMSC-EV−free conditioned medium.

cMSC-sEVs From Post-MI Heart Carry Cytokines With Protumorigenic Properties

EVs encapsulate various cytokines that might contribute to neoplastic growth.[34,35] Compared with cMSC-sEVs from sham-MI hearts, cMSC-sEVs from post-MI hearts carried higher amounts of cytokines involved in the pathogenesis of cardiovascular diseases and cancer,[36] including periostin (3×), osteopontin (2.7×), interleukin-6 (IL-6; 4×), galectin-3 (6.2×), TNFα (tumor necrosis factor α; 1.4×), and VEGF (vascular endothelial
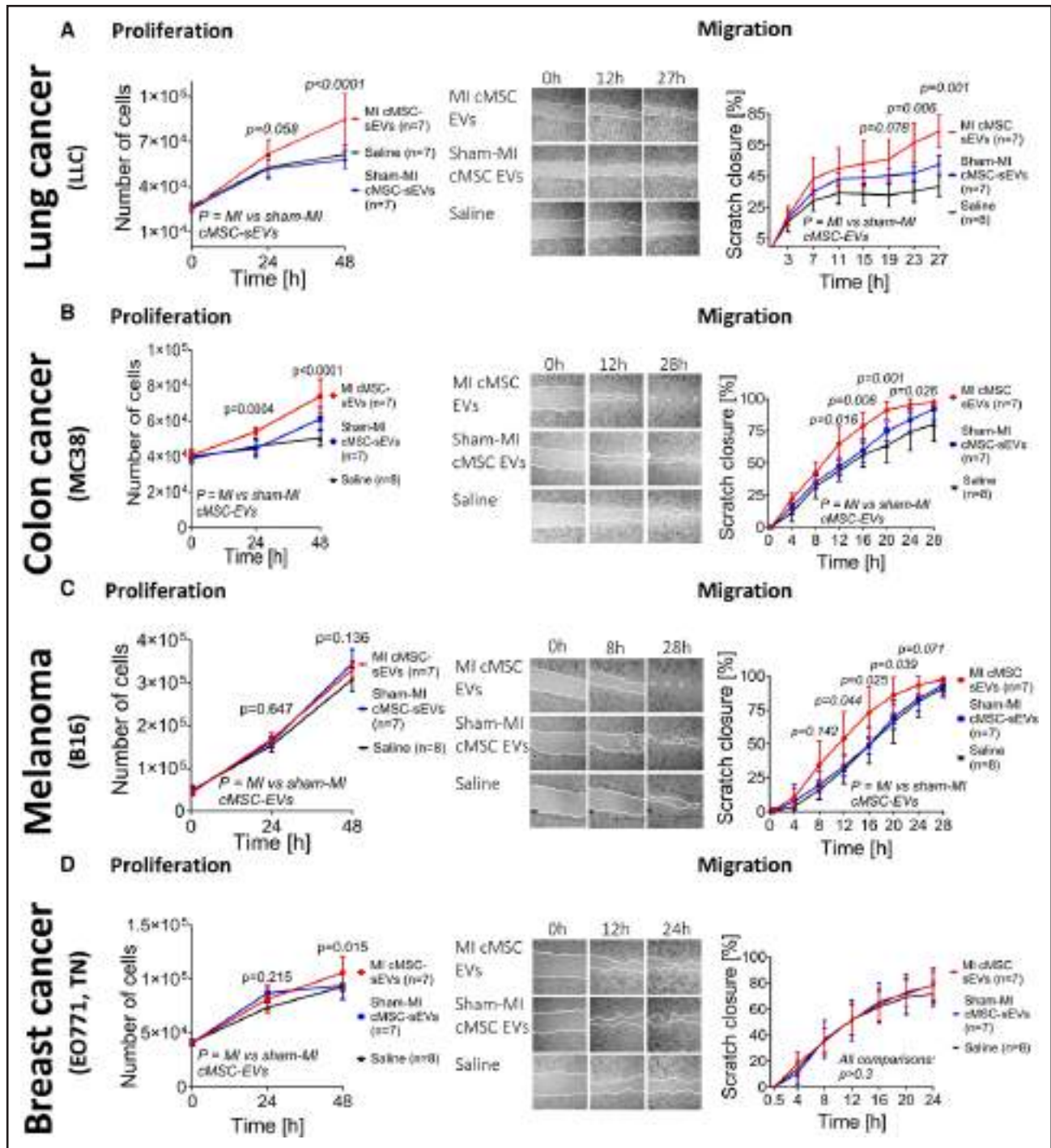
Figure 2. Effects of cMSC-sEVs from post-MI failing hearts on cancer cell proliferation and migration.
cMSC-sEVs were purified 10 days after MI or sham-MI using size exclusion chromatography. The effects of cMSC-sEVs on cancer cell lines were evaluated by colorimetric cell proliferation and cell migration (scratch) assays. **A**, cMSC EVs (10^8 EVs/mL) from post-MI hearts facilitated LLC cancer cell proliferation. *P* for cMSC-sEVs <0.0001, *P* for time <0.0001, and *P* for interaction=0.0001. cMSC-sEVs from post-MI hearts doubled lung cancer cell migration compared with sham-MI cMSC-sEVs. *P* for cMSC-sEVs=0.0002, *P* for time <0.0001, and *P* for interaction=0.0001. Data are expressed as mean±SD. All samples were assayed in duplicate. **B**, cMSC-sEVs (10^9 EVs/mL) from post-MI hearts facilitated MC38 cancer cell proliferation. *P* for cMSC-sEVs <0.0001, *P* for time <0.0001, and *P* for interaction <0.0001. cMSC-sEVs from the post-MI hearts increased MC38 migration compared with sham-MI cMSC-sEVs. *P* for cMSC-sEVs=0.0003, *P* for time <0.0001, and *P* for interaction=0.0001. **C**, cMSC-sEVs accelerated migration but not the proliferation of B16 Melanoma cells. A colorimetric proliferation assay showed that cMSC EVs (10^9 EVs/mL) from post-MI hearts did not facilitate B16 cell proliferation. *P* for cMSC-sEVs=0.8473, *P* for time <0.0001, and *P* for interaction=0.6641. For migration assay: *P* for cMSC-sEVs=0.0059, *P* for time <0.0001, and *P* for interaction=0.0001. **D**, The effect of cMSC-sEVs (10^9 EVs/mL) on proliferation (modest) and migration (no effect) of EO771 breast cancer cells: *P* for cMSC-sEVs=0.0211, *P* for time <0.0001, and *P* for interaction=0.0164; and scratch (migration) assay with 10^9 EVs/mL. *P* for cMSC-sEVs=0.0952, *P* for time (*Continued*)

Figure 2 Continued. <0.0001, and *P* for interaction=0.5765. All samples were assayed in duplicate. Data are expressed as mean±SD. *P* values were calculated using 2-way ANOVA with the Holm-Šídák post test for proliferation assays and repeated-measures 2-way ANOVA with the Holm-Šídák post test for migration assays. *P* for left ventricular dysfunction cMSC-sEVs vs sham-MI cMSC-sEVs is indicated on the graph. cMSC indicates cardiac mesenchymal stromal cells; EV, extracellular vesicle; LLC, Lewis lung cancer; MI, myocardial infarction; and sEVs, small extracellular vesicles.

growth factor; 1.7×; Figure 1J). The concentration of sEV-encapsulated galectin-3, a protein implicated in the pathogenesis of cardiovascular disease and cancer,[36] was 3.5 times higher than that of soluble galectin-3 (Figure 1J; Figure S5B). Post-MI LVD did not affect the amount of IL-1α, IL-1β, IFNγ (interferon-γ), and TGF-β (transforming growth factor β) within cMSC-sEVs (Figure 1J; Figure S5A and S5B). However, the concentration of TGF-β within cMSC-sEVs was 31× higher than that of free TGF-β (Figure 1J; Figure S5B). This finding is noteworthy because TGF-β has been implicated in cancer cell invasion, dissemination, and recruitment of tumor-associated macrophages (TAMs).[37,38]

In parallel, analysis of soluble cytokines in the cMSC-conditioned medium revealed higher quantities of soluble cytokines than cMSC-sEVs (Figure S5B). However, only periostin and IL-6 maintained a higher profile, similar to cMSC-sEVs from post-MI hearts. Our results collectively indicated that cMSC-sEVs from post-MI hearts carried a unique tumor-promoting cytokine signature. Compared with soluble cytokines, the cargo of cMSC-sEVs better reflected the pathological processes within post-MI failing myocardium.

cMSC-sEVs Encapsulated MicroRNAs With Protumorigenic Properties

Protumorigenic microRNAs (miRs) are significantly enriched in sEVs.[16] To determine whether cMSC-EVs carry tumor-promoting miRs, we first analyzed the proteomic profile of LLC tumors from mice with and without post-MI LVD. On day 30 after tumor inoculation, tumor tissues were processed for proteomics. We identified 4909 tumor proteins, of which 101 were differentially expressed in the post-MI LVD group (Figure S6A). Using the TargetScan tool,[39] we identified 48 genes encoding proteins with a known miR binding site in their 3′-untranslated region and a total of 70 miRs that can bind to those sites. Then, to filter for miR with reported involvement in cancer, we used the miRBase tool. We filtered the list for miR involvement in cardiovascular diseases and found 17 potential tumor-promoting miRs (Figure S6B).

We next extracted and analyzed total RNA from cMSC-sEVs. Compared with sham-MI sEVs, cMSC-sEVs from the failing heart contained more tumor-promoting miRs, such as miR-221, that stimulate tumor development, cancer cell proliferation, and migration (Figure 1K). Other miRs that were found more abundantly in cMSC-sEVs from the failing hearts included miR-21, miR-24-1, and miR-214 (Figure 1K). Other tumor-promoting miRs

that were detected in similar amounts in cMSCs-EVs from post-MI LVD and sham-MI included miR-34a and miR-219-5p. Overall, cMSC-sEVs from the failing heart carry higher amounts of specific tumor-promoting miRs.

## cMSC-sEVs From Post-MI Heart Accelerated Proliferation and Migration of Cancer Cells

Activated MSCs possess proneoplastic properties.[27,29] To evaluate the proneoplastic properties of cMSC-sEVs, we added cMSC-sEVs (10^8 EVs/mL) or saline to various cultured cancer cells: LLC lung cancer, MC38 colon cancer, EO771 breast cancer, and B16 melanoma cell lines. Colorimetric-based proliferation assay showed that cMSC-sEVs from post-MI hearts stimulated the proliferation of LLC and MC38 cells by 1.5 and 1.2× more than cMSC-sEVs from sham-MI hearts or saline (Figure 2A and 2B, left column). The proliferative effect of cMSC-sEVs corresponded to a dose-response pattern (Figure S7A and S7B). Overall, the effects of cMSC-sEVs were tumor-specific: significant on lung and colon cancer cells and modest or null with breast and melanoma cancer cells (Figure 2A through 2D, left column).

Next, using a scratch assay, we assessed the effect of cMSC-sEVs on migration of cancer cells (Figure 2, middle column). Administration of cMSC-sEVs (10^7 EVs/mL) from post-MI hearts accelerated migration of LLC cells compared with cMSC-sEVs from sham-MI or saline (Figure 2A, right column). The magnitude of the effect increased as the concentration of EVs increased (Figure S7C and S7D). It is surprising that the migratory effect on LLC cells decreased with the highest concentration of cMSC-sEVs. Next, we found that cMSC-sEVs from the post-MI hearts accelerated migration of MC38 (colon) and B16 (melanoma), but not EO771 (breast) cancer cell lines (Figure 2B through 2D, right column). Overall, compared with lung and colon cancers, melanoma and breast cancer cell lines were less affected by post-MI cMSC-sEVs.

Finally, ECs have been implicated in the development and progression of tumors.[33] We found that cMSC-sEVs from the post-MI heart (10^9 EVs/mL) promoted C166 EC permeability and migration (Figure S7E and S7F).

cMSC-sEVs Switched Macrophages Into a Protumorigenic Phenotype

Monocytes and macrophages, whose functions could be regulated by sEVs,[20] have both tumor-promoting and tumor-suppressive effects.[37,40] To determine the effect of
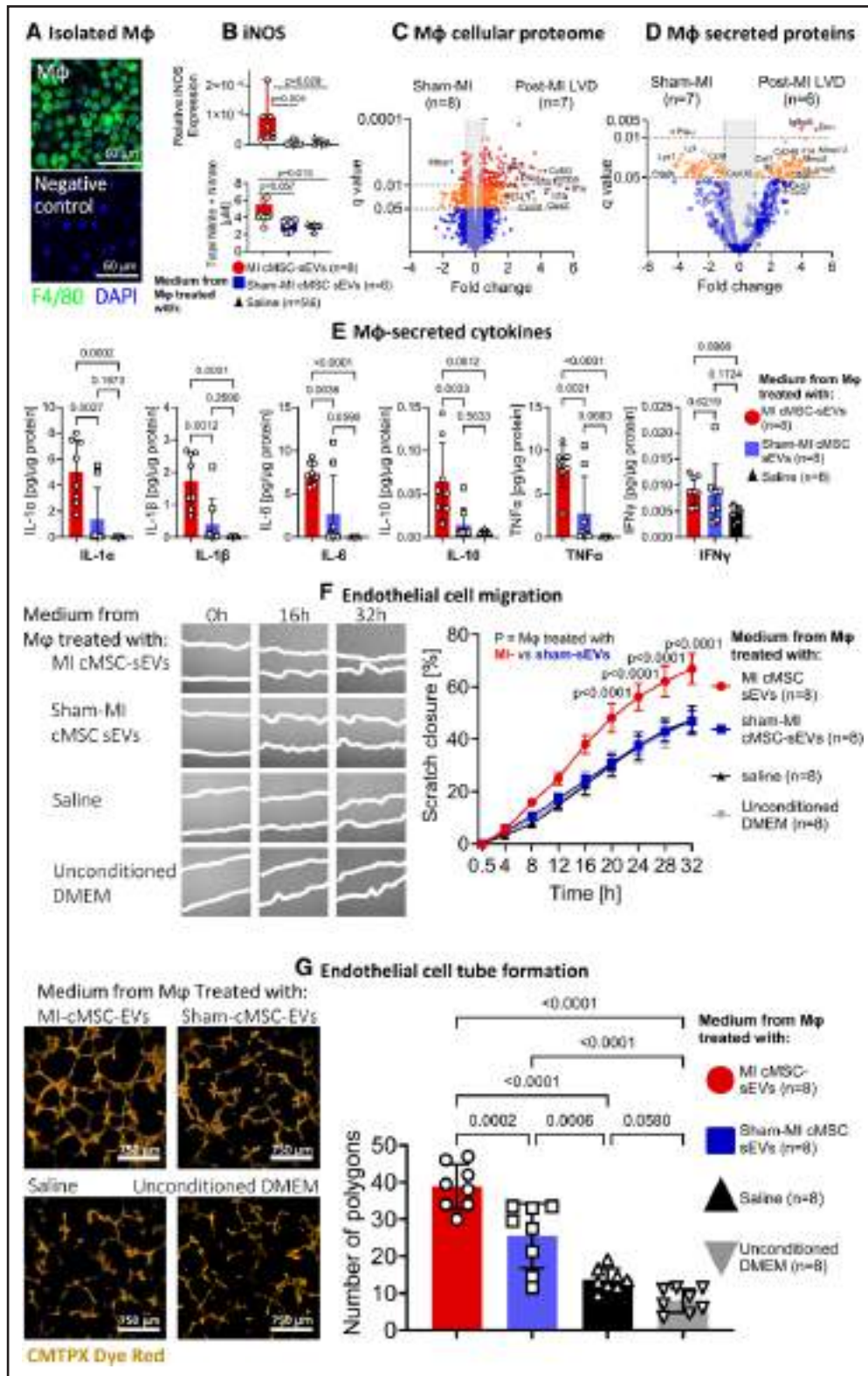
Figure 3. cMSCs from post-MI failing hearts switched macrophages into a tumor-promoting phenotype.
A, To study the effect of cMSC-sEVs on macrophage activation, we isolated peritoneal macrophages from female C57BL/6 mice using a resistance to trypsinization assay. The purity of isolated macrophages reached 96% by staining for F4/80 and DAPI. Scale bars=60 nm. **B**, To assess the activity of iNOS (inducible nitric oxide synthase) in cMSC-sEV–treated macrophages, we incubated macrophages with cMSC-sEVs (10^9 EVs/mL) from the post-MI heart, sham-operated heart, or saline for 24 hours in serum-free conditions. Then, cells were washed and incubated for another 24 hours in a serum-free medium. After 24 hours, we collected the macrophage-conditioned medium and isolated total macrophage RNA. We used reverse transcription polymerase chain reaction to determine the expression iNOS in isolated (*Continued*)

Figure 3 Continued. macrophages and measured the total concentration of nitrite and nitrate in the conditioned medium of incubated macrophages. Expression of both iNOS was upregulated after incubation with cMSC-sEVs from post-MI hearts and the concentration of nitrites and nitrates in conditioned medium. Data are expressed as mean±SD. *P* values were determined by the Kruskal-Wallis test with the Dunn post test. *P* for iNOS=0.0003 and *P* for nitrites and nitrates=0.004. *P* values for specific comparisons are displayed on the graph. **C** and **D**, We incubated macrophages with cMSC-sEVs (109 EVs/mL) from the post-MI heart, sham-operated heart, or saline for 24 hours in serum-free conditions. Then, cells were washed and incubated for another 24 hours in a serum-free medium. After 24 hours, we collected the macrophage-conditioned medium and lysed the macrophages. The proteomes of macrophages lysate (**C**) and conditioned medium (**D**) were analyzed to assess cellular and extracellular proteome. *P* values were determined by using a *t* test multiple times with multiple testing corrections (false discovery rate correction). **E**, We used ELISA assays to determine whether cMSC-sEVs from post-MI LVD modulate macrophage cytokine secretion. *P* values were determined by 1-way ANOVA with the Holm-Šídák post test to account for multiple comparisons. Data passed the D'Agostino-Pearson normality test. **F** and **G**, cMSC-sEVs from post-MI mice (10^9 EVs/mL) switched macrophage into a proangiogenic phenotype. To assess the proangiogenic properties of conditioned medium from cMSC-EV–treated macrophages, we conducted a tube formation assay. C166 endothelial cells were stained with Cell TrackerTM Red CMTPX Dye according to the manufacturer protocol. First, the conditioned medium from macrophages treated with post-MI cMSC-sEVs accelerated migration of the C166 endothelial cell line, compared with cMSC-sEVs from sham-MI, demonstrated by a scratch closure assay (**E**). *P* values were calculated using repeated-measures 2-way ANOVA with the Holm-Šídák post test. *P* for LVD cMSC-sEVs <0.0001, *P* for time <0.0001, and *P* for interaction <0.0001. *P* for post-MI cMSC-sEVs vs sham-MI cMSC-sEVs is displayed on the graph. Next, cMSC-sEVs from post-MI mice (10^9 EVs/mL) stimulated macrophages to induce tube formation in angiogenesis assay with C166 endothelial cells (**G**). Scale bar=750 μm. Data are expressed as mean±SD. *P* values were determined by 1-way ANOVA with the Holm-Šídák post test (*P*<0.0001). Data passed the D'Agostino-Pearson normality test. *P* values for specific comparisons are indicated on the graph. cMSC indicates cardiac mesenchymal stromal cell; DAPI, 4′,6-diamidino-2-phenylindole; EV, extracellular vesicle; IFNγ, interferon-γ; IL, interleukin; LVD, left ventricular dysfunction; MI, myocardial infarction; sEVs, small extracellular vesicles; and TNFα, tumor necrosis factor α.

cMSC-sEVs on macrophage activation and function, we isolated peritoneal macrophages from naive mice (96% purity; Figure 3A).[41] Adding cMSC-sEVs from post-MI failing heart, sham-operated heart, or saline, we found that cMSC-EVs from the post-MI heart upregulated the expression of iNOS (inducible nitric oxide synthase; Figure 3B, top). Moreover, concentrations of nitrite and nitrate, indirect products of iNOS, were higher in the conditioned medium of macrophages treated with sEVs from post-MI heart (Figure 3B, bottom). These findings are significant because TAMs are characterized by producing NO and reactive oxygen intermediates that can cause DNA damage and genetic instability during the initiation phase of tumors.[37]

To further characterize the changes in macrophages after cMSC-sEVs exposure, we analyzed cellular and extracellular macrophage proteins (Figure 3C and 3D). Comparative proteomics of cellular macrophage proteins revealed that cMSC-sEVs from the post-MI heart–enriched pathways related to inflammation, immune modulation, angiogenesis, and remodeling of the extracellular matrix (Figure 3C; Figure S8A through S8H). Activated macrophages upregulated the expression of the immune-checkpoint molecule PD-L1 (programmed death-ligand 1) at mRNA (Figure S8I) and proteomic levels (Figure S8E). PD-L1 induces inactivation and apoptosis of cytotoxic T lymphocytes and thus promotes immune suppression and tumor growth. It is significant that PD-L1 expression is an established characteristic of TAMs.[37,42]

Proteomics of macrophage-conditioned medium revealed that cMSC-EVs from post-MI LVD induced significant changes in the profile of macrophage-secreted proteins (Figure 3D; Figure S9A and S9B). These changes included upregulation of proinflammatory cytokines and chemokines, proangiogenic mediators, and downregulation in antiangiogenic proteins (Figure S9C and S9E). Biological pathway analysis revealed enrichment in processes related to tumor formation, inflammation, angiogenesis, and extracellular matrix remodeling, and depletion in processes related to the regulation of proliferation and cell death (Figure S9F and S9G). Together, macrophage proteome indicated that cMSC-EVs from post-MI heart educated macrophages into a protumorigenic state with many characteristics of TAM.[17]

Cytokines are among the most significant messengers and effectors in executing macrophage functions.[34,35] Cytokine array revealed that macrophages exposed to post-MI cMSC-sEVs secreted higher amounts of cytokines implicated in the pathogenesis of cardiovascular diseases and cancer, namely IL-1α and β, IL-6, IL-10, and TNFα (Figure 3E).[36] Thus, cMSC-sEVs from post-MI LVD educated macrophages to express a unique cytokine profile with protumorigenic properties.

Proangiogenic macrophages contribute to tumor angiogenesis, growth, and metastasis.[37] We found that conditioned medium from post-MI cMSC-sEV–educated macrophages stimulated EC migration (Figure 3F) and enhanced angiogenesis by EC tube formation assay (Figure 3G).

Finally, we studied whether macrophages educated by cMSC-EVs from post-MI hearts modulate proliferation or migration of lung (LLC) and colon (MC38) cancer cells. We found that conditioned medium from educated macrophages did not affect the proliferation and migration of LLC cells in vitro (Figure S10A and S10B) but slightly reduced MC38 cell proliferation and did not affect migration (Figure S10C and S10D). cMSC-sEVs originating from post-MI cardiac tissue collectively induce macrophages to adopt proangiogenic, proinflammatory, and immune-modulating characteristics that could, in turn, support tumor growth.
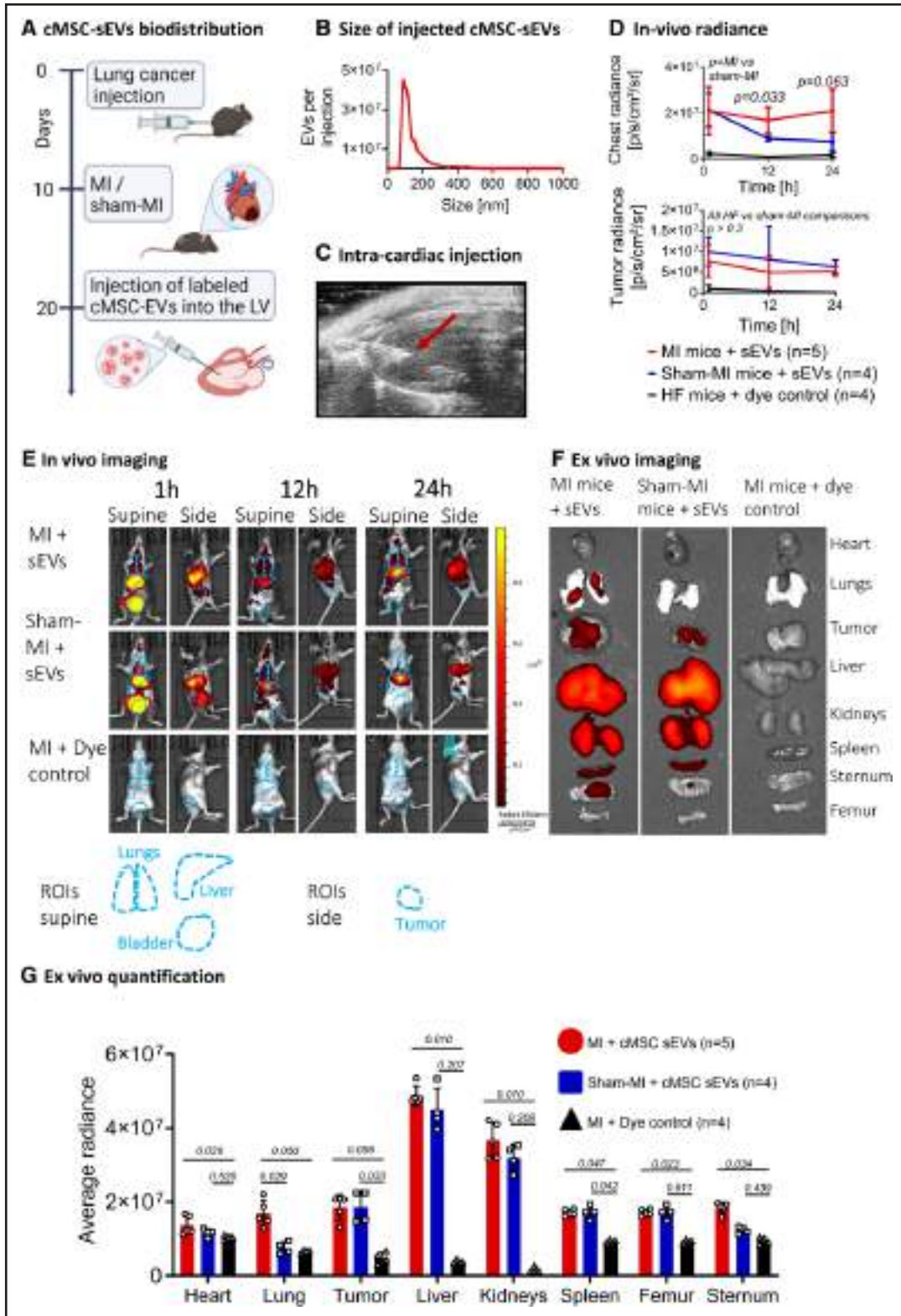
Figure 4. Biodistribution and uptake of cMSC-sEVs.
A, To evaluate the biodistribution of cMSC-sEVs, we used IVIS Lumina LT for both in vivo and ex vivo imaging. We isolated cMSC-sEVs from donor mice 10 days after MI, labeled them with near-infrared dye, and injected them into the LV cavity of tumor-bearing recipient mice after either MI or sham-MI. We used the same amount of dye for control in a sample without sEVs. **B**, Size distribution of injected cMSC-sEVs from post-MI LVD mice was in the small EV range. **C**, Representative image for echocardiography-guided LV cavity injection of labeled EVs. The red arrow points to the needle. We confirmed the success of the injection by echocardiography imaging of a bubble jet in the LV cavity during injection. **D**, Quantification of the fluorescence activity of cMSC-sEVs in vivo. We quantified the radiance of the chest and the tumor area 1, 12, and 24 hours after injection. We found that post-MI LVD enhanced the retention of cMSC-sEVs in the area of the lungs. In addition, we found (*Continued*)

Figure 4 Continued. fluorescence activity in the tumor area of both post-MI LVD and sham-MI mice. Data are expressed as mean±SD. *P* values were calculated using repeated-measures 2-way ANOVA with the Holm–Šídák post test. For the retention in the lungs: *P* for post-MI LVD=0.0001, *P* for time=0.0785, *P* for interaction=0.1357. For the retention in the tumors: *P* for post-MI LVD=0.0003, *P* for time=0.2685, *P* for interaction=0.9263. *P* for post-MI LVD vs sham-MI is displayed on the graph. **E**, Representative images of fluorescence activity in mice with and without post-MI LVD after injection of labeled cMSC-sEVs from post-MI LVD mice. Post-MI LVD facilitated the distribution and retention of cMSC-sEVs in the lungs, and we detected fluorescence activity in the tumor area of both post-MI LVD and sham-MI mice. Outlines of the lungs, liver, bladder, and tumor are depicted in dotted light blue lines. **F**, To reduce background fluorescence, enhance fluorescence signal, and evaluate the distribution of cMSC-sEVs from post-MI LVD mice to specific organs, we performed ex vivo analysis 24 hours after cMSC-sEVs injection. The highest signal was detected in the liver and kidneys, and an intermediate signal was detected in the tumor and spleen. Furthermore, we confirmed our in situ findings and showed that post-MI LVD promoted cMSC-sEV distribution to the lungs. **G**, Quantification of the fluorescence activity of cMSC-sEVs ex vivo. We quantified the radiance of the heart, lungs, tumor, liver, kidneys, spleen, sternum, and femur 24 hours postinjection. *P* values were calculated using Kruskal-Wallis with the Dunn post test. Data are expressed as mean±SD. *P* for heart=0.024, lungs=0.003, tumor=0.008, liver=0.002, kidneys=0.002, spleen=0.009, sternum=0.017, and femur <0.0001. *P* values for post test comparisons are displayed in the graph. cMSC indicates cardiac mesenchymal stromal cell; EV, extracellular vesicle; HF, heart failure; LV, left ventricle; LVD, left ventricular dysfunction; MI, myocardial infarction; ROI, region of interest; and sEVs, small extracellular vesicles. Illustration created with BioRender.com.

Biodistribution and Uptake of cMSC-sEVs

Tracking in vivo destination of cEVs is essential for understanding their contribution to tumor growth. To assess the distribution of cMSC-sEVs in vivo, we used a mouse model of adoptive transfer. We first labeled cMSC-sEVs from MI hearts with a near-infrared spectroscopy fluorescent dye. Next, we injected the labeled cMSC-sEVs systematically into the LV cavity of mice 10 days after MI or sham-MI, bearing heterotopic LLC tumors (Figure 4A through 4C) and assessed the distribution of cMSC-sEVs by bioluminescent IVIS Spectrum imaging. We found increased fluorescent activity in situ in the chest of post-MI mice compared with sham-MI mice (Figure 4D and 4E). Next, to improve the signal and reduce interferences, we ex vivo scanned the internal organs, including tumors, 24 hours after injection (Figure 4F and 4G). We found enhanced fluorescent activity of sEVs in the liver, kidneys, lungs, spleen, bones, and tumors (Figure 4F and 4G).

After MI, the accumulation of post-MI LVD cMSC-sEVs in the congested lungs was greater than in the lungs of sham-MI mice (Figure 4F and 4G). Together, our biodistribution studies indicated that cMSC-sEVs biodistributed to various organs and tumors. Post-MI LVD promoted cMSC-sEV accumulation in congested lungs.

cMSC-sEVs From the Post-MI Heart Accelerated the Growth of Heterotopic Lung Tumor
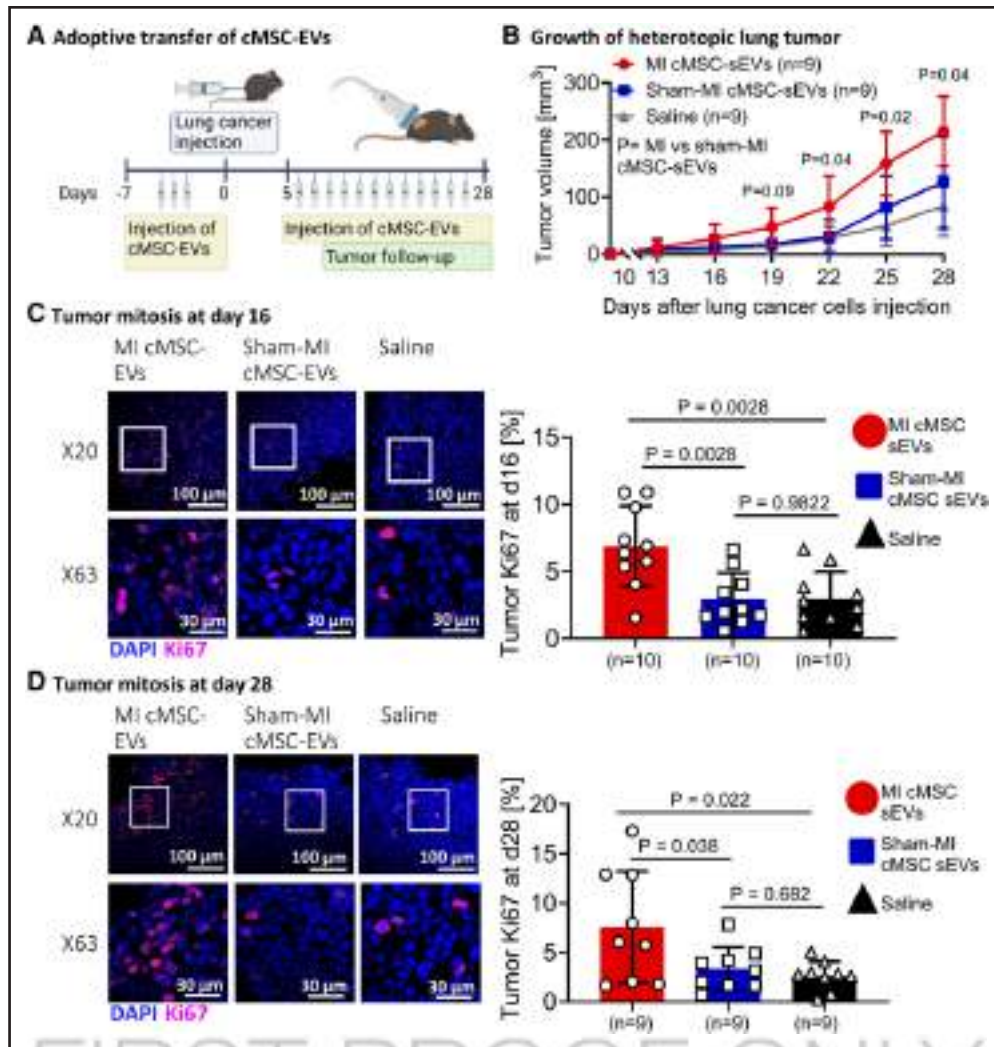
To dissect the effect of cMSC-sEVs from other factors released from the post-MI failing heart, we used a model of adoptive transfer of cMSC-sEVs to LLC tumor-bearing mice with normal hearts (Figure 5A). We subcutaneously injected cMSC-sEVs (2 µg of EV protein; Figure S11A) or saline into the cancer cell inoculation site. We found that transfer of cMSC-sEVs from failing hearts promoted the appearance of visible tumors (Figure S11B). Moreover, cMSC-sEVs from the failing heart accelerated tumor growth compared with sham-MI EVs or saline (Figure 5B). This was confirmed by the heavier tumors in mice treated with cMSC-sEVs from post-MI hearts

(Figure S11C). Finally, histological analysis for expression of Ki67, a marker of cell cycle activity and tumorigenesis, revealed a higher percentage of Ki67 in tumors treated with cMSC-sEVs from the post-MI heart at 16 days, before differences in tumor volumes accelerated (Figure S11C through S11E), and 28 days after tumor inoculation (Figure 5C and 5D; Figure S11C and S11D). We found mechanistically that the percentage of Ki67 correlated with tumor volume at day 28, but not at day 16 (Figure S11F and S11G). Thus, changes in tumor cell proliferation preceded the acceleration in tumor growth. Overall, cMSC-sEVs from the post-MI heart stimulated tumor cell proliferation and growth.

EV Depletion Reduced the Tumor-Promoting Effects of Post-MI LVD

Interfering with EV secretion and uptake reduces tumor growth, impedes metastatic progression, and inhibits the systemic effects of cancer.[16] To determine whether EV depletion would reduce the effects of post-MI LVD on tumor growth, we used GW4869, an inhibitor of the enzyme that converts membrane sphingomyelin into ceramide, which is required for the formation of EVs.[43] LLC cells were inoculated to the hindlimb of mice, and 10 days later, mice were randomly assigned for MI or sham-MI. Starting 3 days after MI or sham-MI, mice from each group were further randomly assigned to receive intraperitoneal injections of GW4869 or dimethyl sulfoxide (vehicle) every 48 hours (Figure 6A). We confirmed effective EV depletion in isolated sEVs from the whole heart tissue at the end of the experiment (20 days after MI; Figure 6B). EV depletion significantly attenuated tumor growth after MI (Figure 6C) and, to a lesser extent, after sham-MI (Figure 6C; Figure S12A), suggesting that GW4869 also affects protumorigenic sEVs from sources other than the heart. Still, the marked reduction in tumor growth in post-MI mice during EV depletion suggested that inhibiting cardiac sEVs after MI contributed to reduced tumor growth.

Staining of tumor slides for Ki67 confirmed increased cell cycle activity in tumors from mice with post-MI LVD.

Figure 5. cMSC-sEVs from post-MI failing hearts accelerated growth of heterotopic lung tumor.
A, To dissect the effects of cMSC-sEVs from other soluble factors, we randomly assigned mice to receive an equal amount of cMSC-sEVs from post-MI LVD, sham-MI (2 µg of EV protein), or saline every 48 hours. Each mouse received 3 subcutaneous injections to the inoculation site the week before Lewis lung cancer cell inoculation (750 000 cells in 100 µL of saline) and another 12 injections resuming 5 days after inoculation. **B**, We monitored tumor growth with serial ultrasound examinations. Mice that received subcutaneous injections of cMSC-sEVs from post-MI hearts developed larger tumors than mice treated with sham-MI cMSC-sEVs. Data are expressed as mean±SD. *P* values were determined by repeated-measures 2-way ANOVA with the Holm-Šídák post test. *P* for cMSC-sEVs from LVD=0.0023, *P* for time <0.0001, and *P* for interaction <0.0001. *P* values for LVD cMSC-sEVs vs sham-MI cMSC-sEVs are displayed on the graph. **C** and **D**, To determine whether cMSC-sEVs from the post-MI hearts facilitated cancer cell proliferation, we stained tumor sections for Ki67 and assessed the number of mitoses. We found a higher percentage of mitoses from tumors of mice who received cMSC-sEVs from post-MI hearts, compared with sham-MI cMSC-sEVs or saline. This higher rate of tumor cell mitosis was detected on day 16 (**D**), before any differences in tumor volume, and on day 28 (**C**). Data are expressed as mean±SD. *P* values were determined by 1-way ANOVA with the Holm-Šídák post test. *P* for day 28=0.0154 and *P* for day 16=0.0009. *P* values for specific comparisons are displayed on the graph. Normality was tested using the D'Agostino-Pearson omnibus test. Scale bars=100 µm (**top** stains) and 30 µm (**bottom** stains). cMSC indicates cardiac mesenchymal stromal cells; DAPI, 4′,6-diamidino-2-phenylindole; EV, extracellular vesicle; sEVs, small extracellular vesicles; LVD, left ventricular dysfunction; and MI, myocardial infarction. Illustration created with BioRender.com.

GW4869 significantly reduced the percentage of Ki67 in tumor cells (Figure 6D; Figure S12B). Thus, EV depletion reduced tumor growth, at least in part, by reducing cancer cell proliferation. Moreover, sEV depletion reduced the power of the inverse correlation between LV ejection fraction and tumor volume (Figure S12C). Overall, our data suggested that EV depletion decreases the association between post-MI LVD and neoplastic growth.

The inhibitory effect of the GW4869 on the growth of tumors could be linked to a systemic depletion of EVs (including tumor EVs) and other mechanisms independent of the action of cEVs. To dissect the role of cEVs in accelerating tumor growth and differentiate it from EVs from other sources, we created a new model of systemic EV depletion with transfer of cMSC-sEVs in mice with post-MI LVD (Figure 6E). Again, GW4869 depleted EVs in the heart (Figure S12D and S12E), and although
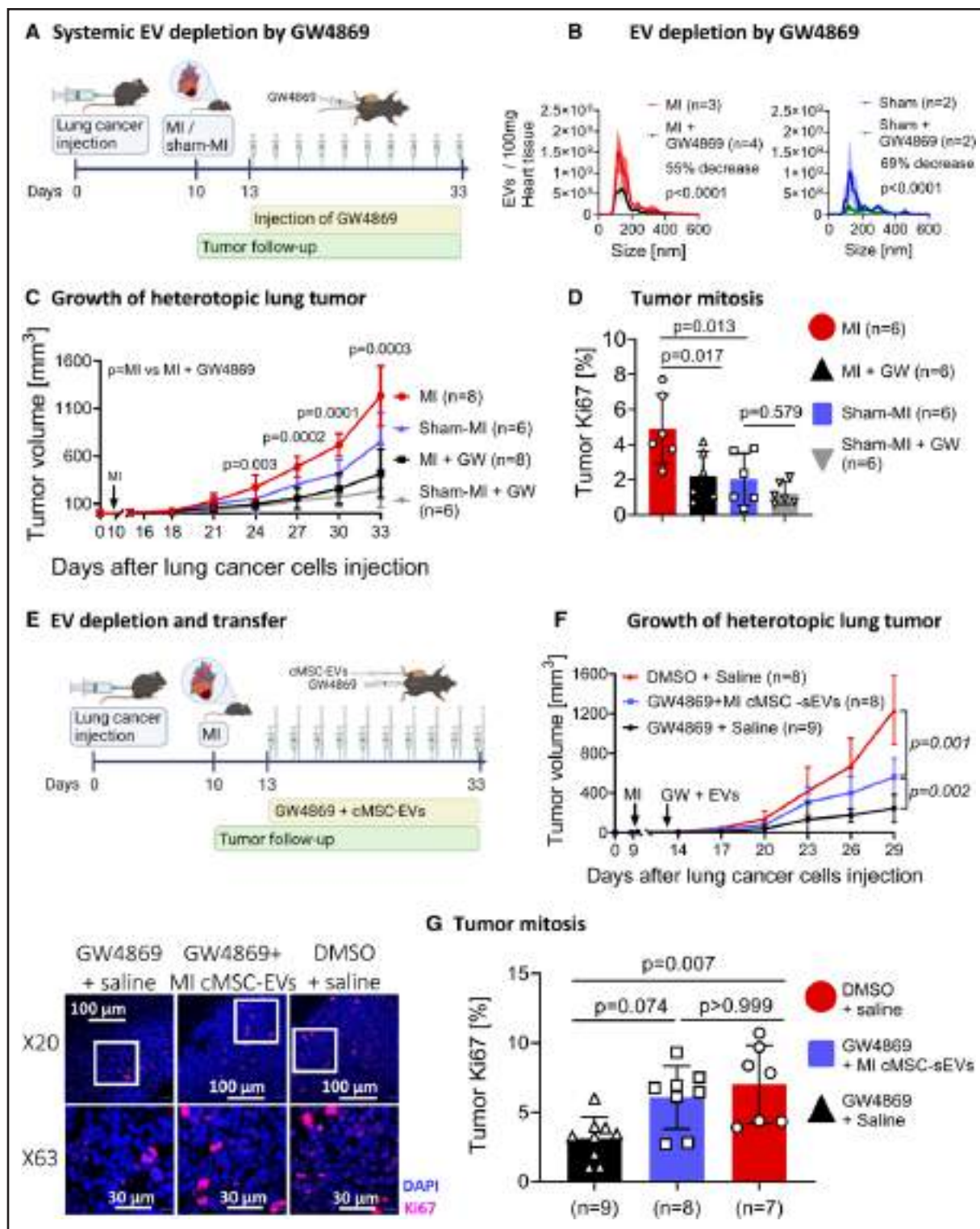
Figure 6. Systemic sEV depletion attenuated heterotopic lung tumor growth and transfer of post-MI cMSC-sEVs restored tumor growth.
A, Lewis lung cancer cells (750 000 cells in 100 μL of saline) were inoculated into the hindlimb of mice. Ten days later, mice were randomly assigned for MI or sham-MI operation. Starting 3 days after MI or sham-MI, mice from each group were further randomly assigned to receive intraperitoneal injections of GW4869 (2.5 mg/kg) or DMSO (GW4869 vehicle as control) every 48 hours. Tumor growth and heart function were assessed by ultrasound and echocardiography. **B**, To validate that intraperitoneal injections of GW4869 depleted cardiac EV production, we separated EVs directly from cardiac tissue and analyzed them with nanoparticle tracking analysis. GW4869 successfully reduced the number of EVs in post-MI hearts (**B**) and sham-MI hearts (**C**). *P* values and percentage change were determined by zero-inflated negative binomial regression. **C**, Mice with post-MI LVD developed larger tumors than sham-MI mice, and EV depletion attenuated the tumortrophic effects of post-MI LVD. Data are expressed as mean±SD. *P* values were determined by repeated-measures 2-way ANOVA with the Holm-Šídák post *(Continued)*

Figure 6 Continued. test. The *P* values for GW4869, for time, and for interaction were <0.0001. Post test *P* values are displayed on the graph for post-MI LVD with vs without GW4869. **D,** To support our findings, we stained the tumors for Ki67 and assessed tumor cell mitoses. We found a higher percentage of mitoses in tumors from mice with post-MI LVD. EV depletion reduced the neoplastic effect of post-MI LVD. *P* value determined with 2-way ANOVA with the Holm-Šídák post test. *P* for GW4869=0.0079, *P* for post-MI LVD=0.0038, and *P* for interaction=0.1266. **E,** Transfer of cMSC-sEVs during systemic EV depletion. We inoculated Lewis lung cancer cells (750 000 in 100 μL of PBS) in female C57BL/6 mice and subjected them to MI 10 days later. Three days after MI, we randomly assigned the tumor-bearing mice to 3 treatment groups: (1) GW4869 (2.5 mg/kg IP), and then 2 μg of cMSC-sEVs from the post-MI heart, subcutaneous above the tumor (n=8) every 48 hours; (2) GW4869 (2.5 mg/kg IP) and saline (n=8) every 48 hours; or (3) DMSO (the vehicle of GW4869 as control) and saline (n=8) every 48 hours. We monitored cardiac function and tumor volume with echocardiography and ultrasound. **F,** Transfer of cMSC-sEVs from post-MI hearts restored tumor growth despite systemic EV depletion. Data are expressed as mean±SD. *P* values were determined by repeated-measures 2-way ANOVA with the Holm-Šídák post test. *P* for LVD cMSC-sEVs, for time, and for interaction were <0.0001. *P* for specific post test comparison is indicated on the graph. **G,** We stained tumor sections for Ki67 and assessed tumor cell mitosis. We found that transfer of cMSC-sEVs from the post-MI hearts increased the number of mitoses in the tumor despite systemic EV depletion. Data are expressed as mean±SD. *P* value was determined by Kruskal-Wallis (*P*=0.0063) and Dunn post test. *P* values for specific comparisons are indicated on the graph. Scale bars=100 μm (**top** stains) and 30 μm (**bottom** stains). cMSC indicates cardiac mesenchymal stromal cell; DAPI, 4′,6-diamidino-2-phenylindole; DMSO, dimethyl sulfoxide; EV, extracellular vesicle; GW, GW4869; LVD, left ventricular dysfunction; MI myocardial infarction; and sEVs, small extracellular vesicles. Illustration created with BioRender.com.

---

systemic EV depletion suppressed LLC tumor growth, transfer of cMSC-sEVs from the post-MI heart reaccelerated tumor growth after MI (Figure 6F; Figure S12F). The percentage of Ki67-positive cells in tumor sections (Figure 6G) confirmed the protumorigenic effects of cMSC-sEVs. We thus showed that cMSC-sEVs contribute to the tumor-promoting effects of post-MI LVD independently of EVs from other sources.

cMSC-sEVs Promoted Growth of Orthotopic Lung Tumors

Studying cancer in its natural environment can provide unique insights into tumor biology, tumor-host interactions, and the factors influencing tumor progression. Thus, we performed orthotopic LLC cell transplantation, injecting luciferase-expressing LLC cells into the tail vein of mice, and tracked the spreading LLC cells into the lungs.[9] We assessed tumor spreading and growth by bioluminescence and microcomputed tomography imaging, with and without a nanoparticle-based approach, using glucose-functionalized gold nanoparticles as a metabolically targeted computed tomography contrast agent (glucose coating enhances the uptake by cancer cells).[44]

Consistent with the heterotopic model results, post-MI LVD promoted tumor growth (Figure S13A and S13B). Moreover, we found that cMSC-sEVs from the post-MI LVD hearts accelerated colonization and growth of LLC cells in the lungs of mice after MI (Figure 7A through 7G). Systemic sEV depletion by GW4869 significantly suppressed the tumor-promoting effects of post-MI LVD by a factor of 4.5 (Figure 7C through 7F). Transfer of cMSC-sEVs from post-MI hearts, but not from sham-MI hearts, partially reestablished the tumor-promoting effects of post-MI LVD (Figure 7C through 7G). These findings were supported by computed tomography imaging of lungs with glucose-functionalized gold nanoparticles (Figure S14A and S14B). Together, we confirmed and supported our earlier findings that post-MI LVD cMSC-sEVs contributed to tumor growth.

We also established an orthotopic model of breast cancer tumors using the 4T1 cell line implanted in the mammary pad of syngeneic female Balb/c mice (Figure S15A). We found that post-MI LVD accelerated tumor growth modestly (Figure S15B). Furthermore, EV depletion by GW4869 had minimal effect on tumor growth (Figure S15B). Thus, the effect of post-MI LVD and the contribution of cardiac sEVs varied with specific types of cancer.

Post-MI Spironolactone Restrained Tumor Growth

Post-MI LVD is characterized by maladaptive neurohormonal activation, particularly the renin-angiotensin-aldosterone system. To determine whether post-MI LVD treatment by renin-angiotensin-aldosterone system inhibitor would affect cMSC-sEVs and tumor growth, we used spironolactone, an aldosterone receptor antagonist (Figure 8A).[45,46] We found that, although post-MI spironolactone did not improve LV ejection fraction, it attenuated post-MI LV remodeling and improved global longitudinal strain (Figure S16A through S16C). Although post-MI LVD significantly accelerated growth of LLC tumors, spironolactone attenuated this effect (Figure 8B; Figure S16F). Moreover, we found that reduced LV remodeling, as indicated by LV dimension, was correlated with smaller tumor volumes in mice with post-MI LVD (Figure S16D). It is noteworthy that spironolactone treatment did not reduce tumor volume or weight in sham-MI mice (Figure 8B; Figure S16F), suggesting that spironolactone lacked direct antitumor properties. Finally, we found that spironolactone reduced the rate of cell cycle activity (Ki67) in tumor cells in mice with post-MI LVD but not in sham-MI mice (Figure 8C; Figure S16E). Our findings collectively suggest that post-MI spironolactone reduced tumor growth.

To further dissect the effect of post-MI spironolactone on cMSC-sEVs, we assessed the effect of spironolactone treatment on the generation of cMSC-sEVs (Figure 8D).
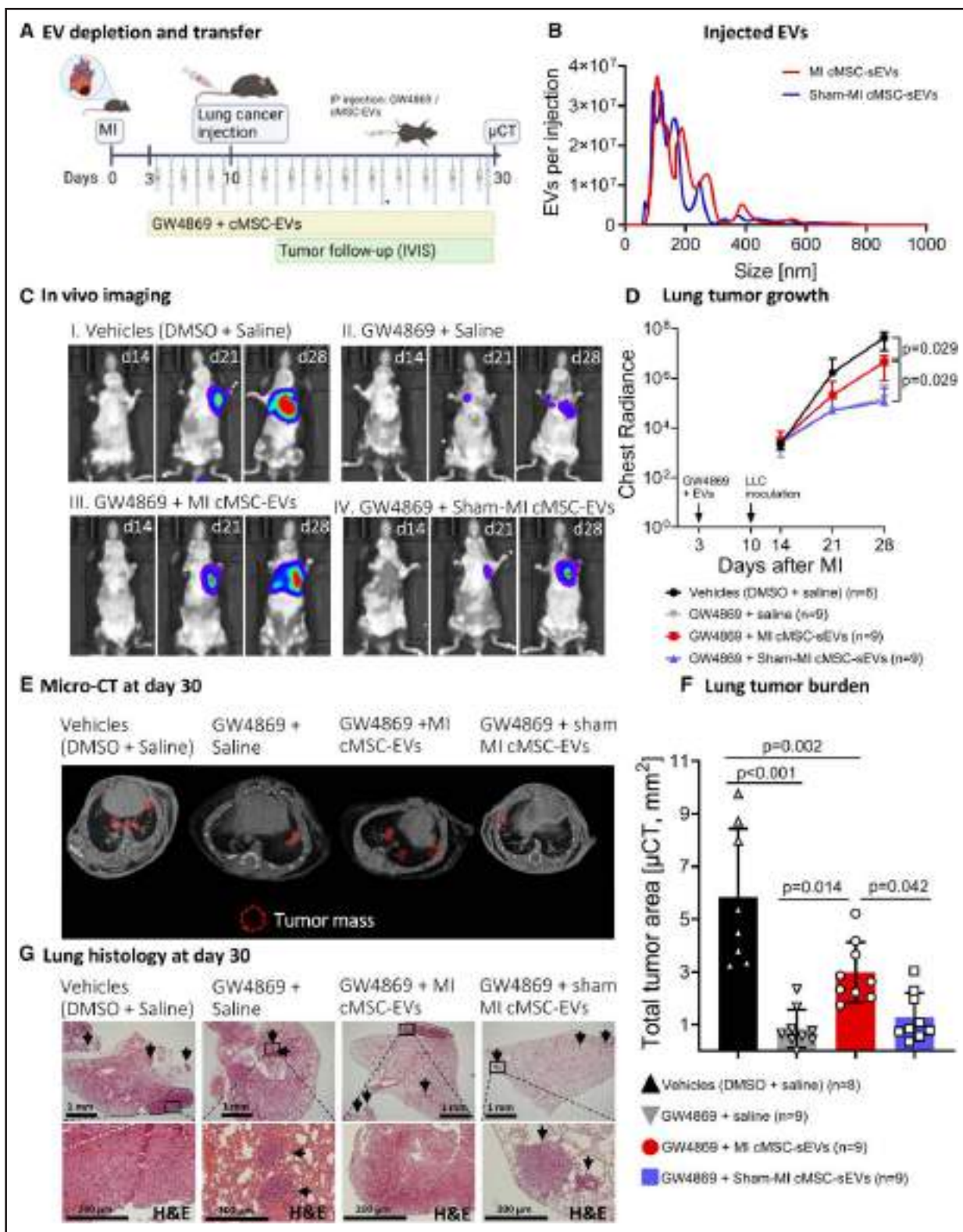
Figure 7. cMSC-sEVs from post-MI failing hearts promoted growth of orthotopic lung tumor.

A, To investigate the role of cMSC-sEVs in the spreading and growth of lung tumors, we used an orthotopic lung cancer model, EV depletion by GW4869, and cMSC-sEV transfer from either post-MI LVD or sham-MI mice. We induced post-MI LVD in female C57BL/6 mice, and 3 days after MI, we randomly assigned the tumor-bearing mice to 4 treatment groups: (1) GW4869 (2.5 mg/kg IP) and then 10 µg of cMSC-sEVs from the post-MI heart intraperitoneally (n=9) every 48 hours; (2) GW4869 (2.5 mg/kg IP) and then 10 µg of cMSC-sEVs from sham-MI intraperitoneally (n=9) every 48 hours; (3) GW4869 (2.5 mg/kg IP) and saline (n=9) every 48 hours; or (4) DMSO (vehicle of GW4869 as control) and saline (n=8) every 48 hours. Treatment with GW4869 started on day 3, and cMSC-sEV transfer started on day 4 to avoid mixing cMSC-sEVs with the GW4869 solution containing DMSO. Then, we injected luciferase-expressing LLC cells (750 000 in 100 µL of PBS) into the tail vein (*Continued*)

Figure 7 Continued. on day 10 after MI. We monitored cardiac function with echocardiography and the development of lung tumors with IVIS on days 14, 21, and 28. In addition, we scanned the lungs with and without injection of glucose-functionalized gold nanoparticles at day 30 using micro-CT. **B**, Size distribution of injected cMSC-sEVs from post-MI LVD or sham-MI mice was mainly in the small EV range. **C**, Representative images of the bioluminescence of the mice at days 14, 21, and 28 after MI. **D**, Quantification of chest bioluminescence after MI and cMSC-sEV transfer. GW4869 reduced the growth of LLC tumors. Transfer of post-MI cMSC-sEVs partially restored accelerated tumor growth. Sham-MI cMSC-sEVs did not affect LLC orthotopic tumor growth. Data are expressed as mean±SD. *P* values were determined by repeated-measures 2-way ANOVA with the Holm-Šídák post test. *P* for post-MI cMSC-sEVs <0.0001, *P* for time <0.0001, and *P* for interaction <0.0001. *P* for post test comparisons indicated on the graph. **E**, Representative images of tumor mass in the lungs by micro-CT at day 30. Individual lung tumors are circled with a dotted red line. **F**, Blinded analysis of total tumor area (tumor burden). cMSC-sEVs from post-MI LVD but not from sham-MI mice promoted the growth of tumor masses in the lungs, even after systemic EV depletion. Micro-CT were was analyzed by a technician blinded to allocating mice into experimental groups. All tumor masses identified in the axial plane were confirmed and discriminated from blood vessels using sagittal and coronal planes. Data are expressed as mean±SD. *P* values by 1-way ANOVA with the Holm-Šídák post test. *P*<0.0001. *P* values for specific post test comparisons are displayed on the graph. **G**, Representative images of lung tumor masses by histological staining for hematoxylin and eosin at day 30. The arrows indicate small lung tumors. The dotted black line circles the larger tumors, and the box outlines the higher-magnification inset below. Scale bars for upper stains (×2 magnification)=1 mm. Scale bars for lower stains (×20 magnification)=200 μm. cMSC indicates cardiac mesenchymal stromal cell; DMSO, dimethyl sulfoxide; EV, extracellular vesicle; sEVs, small extracellular vesicles; H&E, hematoxylin and eosin; LLC, Lewis lung cancer; LVD, left ventricular dysfunction; micro-CT, micro–computed tomography; and MI, myocardial infarction. Illustration created with BioRender.com.

We found that post-MI spironolactone reduced the number of cMSC-sEVs by 28% (Figure 8E). Then, we used a conditioned medium of cMSCs (containing sEVs and soluble proteins) from post-MI hearts with and without spironolactone treatment. We found that, cMSC-conditioned medium, from post-MI hearts treated with spironolactone attenuated LLC cell migration (Figure 8F), but not proliferation (Figure 8G).

Next, we isolated cMSC-sEVs from the conditioned medium and tested equal amounts of cMSC-sEVs from post-MI hearts with and without spironolactone treatment. It was unexpected that equal doses of cMSC-sEVs from post-MI hearts with and without spironolactone treatment had similar effects on LLC migration and proliferation (Figure 8H and 8I). Thus, our data suggest that in vivo antitumor effects of post-MI spironolactone were probably mediated by reducing the number of proneoplastic cMSC-sEVs.

Post-MI spironolactone treatment did not modulate the effects of equal doses of cMSC-sEVs on proliferation and migration of MC38 colon cancer cells (Figure S17A through S17D). Furthermore, compared with no treatment, post-MI spironolactone did not modify the effects of cMSC-sEVs on C166 EC migration (Figure S17E and S17F) and permeability (Figure S17G).

DISCUSSION

Our work provides several new findings. First, we present evidence that post-MI failing hearts, specifically cMSCs, secrete sEVs with protumorigenic properties. cMSC-sEVs transfer multiple factors, including proteins, cytokines, and miRs, that stimulate neoplastic growth and activate protumorigenic macrophages (Figure 8G). Second, the protumorigenic effects of cMSC-sEVs vary with different types of cancers, with lung cancer being the most susceptible. Third, EV depletion reduces the protumorigenic effects of post-MI LVD. Finally, post-MI spironolactone treatment decreases the number of

cMSC-sEVs and suppresses tumor growth. Together, we add a new insight into the evolving field of reverse cardio-oncology with potential clinical implications.

Comparison With Previous Reports

Our work builds on previous studies.[9–11,47] The inflammatory and reparative responses to myocardial injury and failure may promote neoplastic growth by secreting inflammatory, reparative, immunomodulatory, and tumor-promoting mediators. For example, aortic constriction promotes growth of breast and lung tumors in mice.[9] Periostin has been identified as a potentially important mediator, and eliminating plasma periostin abolished the effects on tumor cell proliferation in vitro.[9] However, inhibition of soluble factors, including periostin, has never been studied in vivo. We found that periostin levels were higher in both cMSC-sEVs and cMSC-conditioned medium from post-MI failing hearts. Furthermore, our work identifies other tumor-promoting factors, including cytokines and miRs within cMSC-sEVs. Whether sEVs carry sufficient quantities of cytokines and miRs to prompt changes in cancer cells has been questioned.[16] Here, specific mediators, such as TGF-β, Gal-3, and miRs, were enriched in sEVs. Such mediators can influence tumor progression by promoting premetastatic niche formation and metastasis.[16] Overall, we suggest that, rather than a single factor, multiple factors encapsulated by cMSC-sEVs contribute to the link between heart disease and cancer.

A recent report suggested another mechanism linking sEVs to accelerated tumor growth. In post-MI LVD, plasma sEVs suppress the sensitivity of cancer cells to ferroptosis, an iron-dependent form of apoptosis, thereby promoting tumor growth.[48] The authors proposed that miR-22-3p–enriched EVs from cardiomyocytes are pivotal in this mechanism.[48]

A previous report showed that MI and LVD did not accelerate growth of renal cancer tumors.[47] This finding
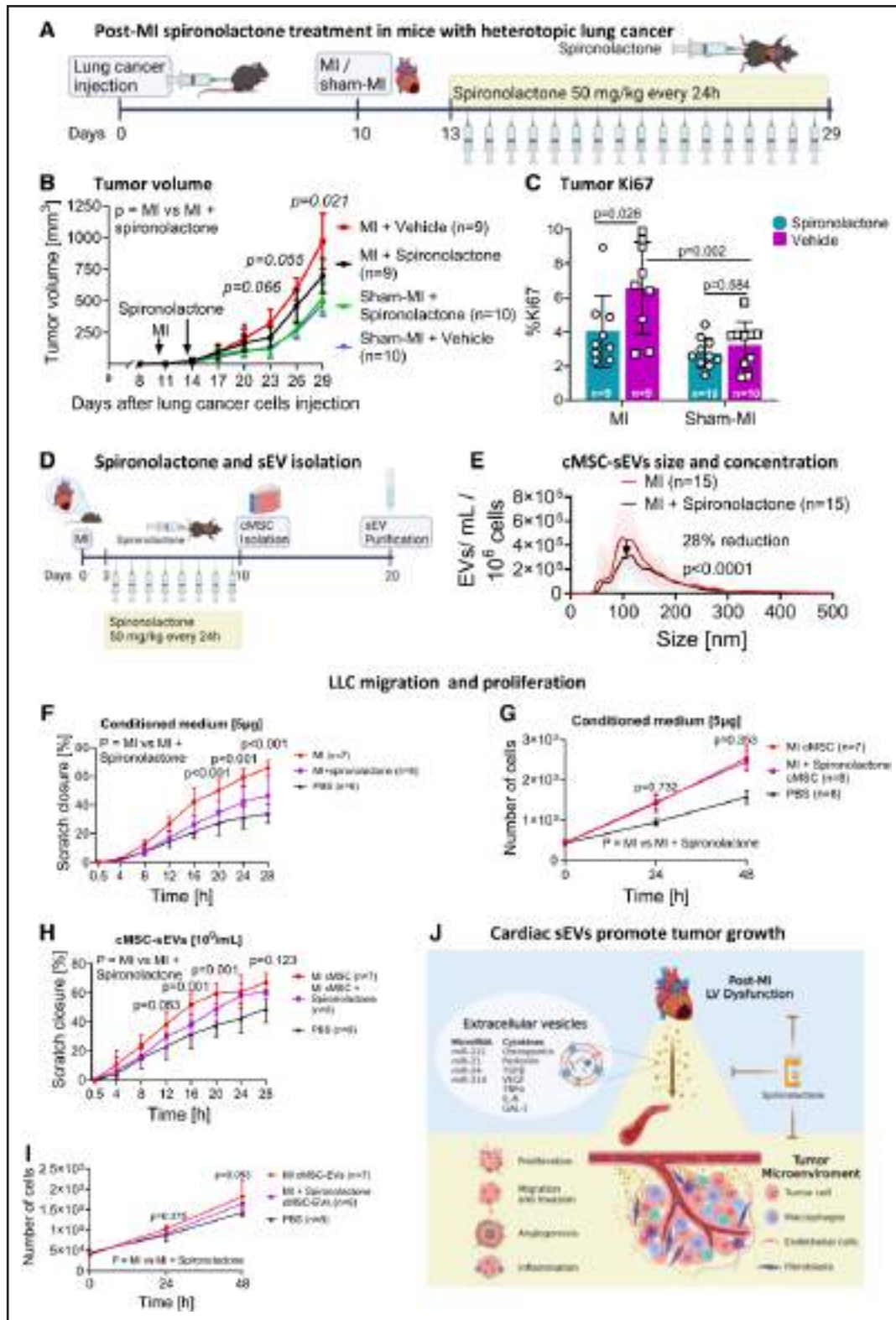
Figure 8. Post-MI spironolactone reduced the tumor-promoting effects of post-MI LVD.
A, We inoculated LLC cancer cells (750 000 in 100 μL of PBS) into female C57BL/6 mice and randomly assigned them to either MI or sham-MI 10 days later. Three days after MI, we started spironolactone treatment (50 mg/kg, daily) or its vehicle, injected subcutaneously. Finally, we performed serial echocardiographic and ultrasound measurements to assess cardiac remodeling, LV function, and tumor growth. **B**, Although post-MI LVD accelerated the growth of heterotopic lung cancer, spironolactone significantly reduced the effect of MI and LVD on tumor growth but had no effect on tumors of sham-MI–operated mice. Data are expressed as mean±SD. *P* values were determined by repeated-measures 2-way ANOVA with the Holm-Šídák post test. *P* for spironolactone <0.0001, *P* for time <0.0001, and *P* for interaction <0.0001. *P* values for post-MI LVD vs post-MI LVD+ spironolactone are displayed on the graph. **C**, To strengthen our findings, we stained the tumors for (*Continued*)

Figure 8 Continued. Ki67 and assessed tumor cell proliferation. We found that spironolactone reduced the number of proliferating cells in tumors from mice with post-MI LVD but had no effect on the tumors of sham-operated mice. Data are expressed as mean±SD. *P* value determined by 2-way ANOVA with the Holm-Šídák post test. *P* for spironolactone=0.018, *P* for post-MI LVD=0.0005, and *P* for interaction=0.0935. *P* values for specific comparisons are displayed on the graph. **D**, To determine whether spironolactone will reduce the number or function of cMSC-sEVs secreted by the post-MI heart, we subjected female C57BL/6 mice to MI. We started spironolactone treatment by subcutaneous injection (50 mg/kg, daily) 3 days later. On day 10, we harvested the hearts and isolated cMSCs. **E**, We purified sEVs from the cMSC-conditioned medium and counted them by nanoparticle tracking analysis. We found that spironolactone reduced sEV release from cMSC by 28%. *P* values and percentage change were determined by zero-inflated negative binomial regression. **F** and **G**, To test the effects of post-MI spironolactone on the function of cMSC-sEVs, we used scratch and proliferation assays. To dissect the effects of cMSC-sEVs from soluble factors, we tested the effects of conditioned medium (5 μg of proteins; **F** and **G**) or purified cMSC-sEVs (10^9/mL; **H** and **I**) on LLC cell migration and proliferation. LLC cell migration was reduced by cMSC-conditioned medium from post-MI hearts treated with spironolactone (**F** and **G**). **H** and **I**, We isolated cMSC-sEVs from the conditioned medium and tested equal amounts of cMSC-sEVs from post-MI hearts with and without spironolactone treatment. Equal dosages of cMSC-sEVs from post-MI hearts with and without spironolactone treatment have similar effects on LLC migration and proliferation. *P* value determined by repeated-measures 2-way ANOVA with the Holm-Šídák post test for migration assays and 2-way ANOVA with the Holm-Šídák post test for proliferation assays. For migration assay with conditioned medium: *P* for spironolactone <0.0001, *P* for time <0.0001, and *P* for interaction <0.0001. For migration assay with purified cMSC-sEVs: *P* for spironolactone <0.0001, *P* for time <0.0001, and *P* for interaction=0.0430. For proliferation assay with conditioned medium: *P* for spironolactone <0.0001, *P* for time <0.0001, and *P* for interaction <0.0001. For proliferation assay with purified cMSC-sEVs: *P* for spironolactone=0.0055, *P* for time <0.0001, and *P* for interaction=0.0166. *P* for post-MI LVD vs post-MI LVD+spironolactone is displayed on the graph. **J**, A schematic presentation describes how cardiac sEVs transmit signals from post-MI failing hearts and accelerate tumor growth. This mechanism could be a target for risk stratification and treatment. Spironolactone treatment reduces the release of cMSC-sEVs and tumor growth. cMSC indicates cardiac mesenchymal stromal cells; EV, extracellular vesicle; GAL, galectin; IL-6, interleukin 6; LLC, Lewis lung cancer; LV, left ventricle; LVD, left ventricular dysfunction; MI, myocardial infarction; miR, microRNA; sEVs, small extracellular vesicles; TGFβ, transforming growth factor-β; TNFα, tumor necrosis factor α; and VEGF, vascular endothelial growth factor. Illustration created with BioRender.com.

agrees with our findings and clinical observations, suggesting that the effects of heart disease on tumor growth cannot be generalized to all types of cancer.

Macrophages play a significant role in tumor initiation, progression, and cytotoxic response.[37,40] Koelwyn et al[11] have shown that MI induced a sustained increase in circulating monocytes that targeted and accelerated tumor growth. Monocyte depletion significantly inhibited tumor growth in mice subjected to MI.[11] Here, we show that cMSC-sEVs from post-MI heart educate macrophages toward the protumorigenic mode. The educated macrophages share specific characteristics with TAM, such as proinflammatory, angiogenic, extracellular matrix remodeling, and immunosuppressive properties.[37] Educated macrophages upregulated the expression of the checkpoint molecule PD-L1, which interferes with the ability of the immune system to eliminate cancer cells and subsequently accelerates tumor growth.

In terms of translation, we show that post-MI spironolactone reduces adverse LV remodeling, the number of cMSC-EVs, and tumor growth. Our findings are significant because they may help to improve the outcome of patients with LVD and cancer. A recent retrospective analysis has shown that renin-angiotensin-aldosterone system inhibitors reduced the rate of mortality and tumor recurrence in hypertensive patients after cancer surgery.[49] Thus, effective LVD therapy may reduce the tumorigenic effects of post-MI LVD.

Limitations and Strengths

First, we used GW4869 to inhibit the production of cEVs. However, GW4869 induces systemic EV depletion and perhaps some other off-target effects.

Moreover, GW4869 may also exert its effects through mechanisms other than EV depletion. However, today, there are no specific, safe inhibitors of EV production, release, or uptake. Still, by cMSC-EV transfer, we demonstrated the independent tumor-promoting effects of cMSC-sEVs in the presence of systemic EV depletion. Second, the methods of infusing sEVs in experimental animals or adding them to cell cultures have been questioned.[18] The administration of exogenous EVs has the limitation of not fully replicating the natural release of cardiac sEVs. However, because the post-MI failing heart secretes additional factors, such as soluble proteins,[9–11] our approach allows us to study and dissect the role of cMSC-sEVs independent of other secreted factors. Third, we have proposed that spironolactone inhibits LLC tumor growth by reducing cMSC-sEV secretion. However, there is a need to determine the precise effect of post-MI spironolactone on the cargo of cMSC-sEVs. Fourth, the detailed mechanisms responsible for the diverse effects of post-MI cMSC-sEVs on the proliferation and migration of different cancer cells is still unclear. Additional research is essential in understanding this phenomenon. Finally, although our results suggest a significant contribution of cMSCs-EVs to tumor growth, we acknowledge the need to investigate the role of sEVs from other cardiac cells in tumor growth.

Summary, Implications, and Future Research

For the first time, we show that cMSCs from post-MI failing heart secrete sEVs that are enriched with multiple protumorigenic factors. Uptake of cMSC-sEVs by cancer cells accelerates tumor growth. Our findings

that post-MI spironolactone attenuated the association between post-MI LVD and tumor growth may have important translational implications. In addition, our results may be relevant to the association between cancer and other cardiovascular diseases, such as atherosclerosis and aortic stenosis. By better understanding the biology and physiology of cardiac sEVs, we may be able to identify new biomarkers and develop more effective treatments for cancer associated with cardiovascular diseases.

REFERENCES

1. Tocchetti CG, Ameri P, de Boer RA, D'Alessandra Y, Russo M, Sorriento D, Ciccarelli M, Kiss B, Bertrand L, Dawson D, et al. Cardiac dysfunction in cancer patients: beyond direct cardiomyocyte damage of anticancer drugs: novel cardio-oncology insights from the joint 2019 meeting of the ESC Working Groups of Myocardial Function and Cellular Biology of the Heart. *Cardiovasc Res*. 2020;116:1820–1834. doi: 10.1093/cvr/cvaa222

2. de Boer RA, Hulot JS, Tocchetti CG, Aboumsallem JP, Ameri P, Anker SD, Bauersachs J, Bertero E, Coats AJS, Celutkiene J, et al. Common mechanistic pathways in cancer and heart failure. A scientific roadmap on behalf of the Translational Research Committee of the Heart Failure Association (HFA) of the European Society of Cardiology (ESC). *Eur J Heart Fail*. 2020;22:2272–2289. doi: 10.1002/ejhf.2029

3. Bertero E, Canepa M, Maack C, Ameri P. Linking heart failure to cancer: background evidence and research perspectives. *Circulation*. 2018;138:735–742. doi: 10.1161/CIRCULATIONAHA.118.033603

4. de Wit S, Glen C, de Boer RA, Lang NN. Mechanisms shared between cancer, heart failure, and targeted anti-cancer therapies. *Cardiovasc Res*. 2023;118:3451–3466. doi: 10.1093/cvr/cvac132

5. Hasin T, Gerber Y, McNallan SM, Weston SA, Kushwaha SS, Nelson TJ, Cerhan JR, Roger VL. Patients with heart failure have an increased risk of incident cancer. *J Am Coll Cardiol*. 2013;62:881–886. doi: 10.1016/j.jacc.2013.04.088

6. Roderburg C, Loosen SH, Jahn JK, Gaensbacher J, Luedde T, Kostev K, Luedde M. Heart failure is associated with an increased incidence of cancer diagnoses. *Esc Heart Fail*. 2021;8:3628–3633. doi: 10.1002/ehf2.13421

7. Banke A, Schou M, Videbaek L, Moller JE, Torp-Pedersen C, Gustafsson F, Dahl JS, Kober L, Hildebrandt PR, Gislason GH. Incidence of cancer in patients with chronic heart failure: a long-term follow-up study. *Eur J Heart Fail*. 2016;18:260–266. doi: 10.1002/ejhf.472

8. Bertero E, Robusto F, Rulli E, D'Ettorre A, Bisceglia L, Staszewsky L, Maack C, Lepore V, Latini R, Ameri P. Cancer incidence and mortality according to pre-existing heart failure in a community-based cohort. *JACC CardioOncol*. 2022;4:98–109. doi: 10.1016/j.jaccao.2021.11.007

9. Avraham S, Abu-Sharki S, Shofti R, Haas T, Korin B, Kalfon R, Friedman T, Shiran A, Saliba W, Shaked Y, et al. Early cardiac remodeling promotes tumor growth and metastasis. *Circulation*. 2020;142:670–683. doi: 10.1161/CIRCULATIONAHA.120.046471

10. Meijers WC, Maglione M, Bakker SJL, Oberhuber R, Kieneker LM, de Jong S, Haubner BJ, Nagengast WB, Lyon AR, van der Vegt B, et al. Heart failure stimulates tumor growth by circulating factors. *Circulation*. 2018;138:678–691. doi: 10.1161/CIRCULATIONAHA.117.030816

11. Koelwyn GJ, Newman AAC, Afonso MS, van Solingen C, Corr EM, Brown EJ, Albers KB, Yamaguchi N, Narke D, Schlegel M, et al. Myocardial infarction accelerates breast cancer via innate immune reprogramming. *Nat Med*. 2020;26:1452–1458. doi: 10.1038/s41591-020-0964-7

12. Jovani M, Liu EE, Paniagua SM, Lau ES, Li SX, Takvorian KS, Kreger BE, Splansky GL, de Boer RA, Joshi AD, et al. Cardiovascular disease related circulating biomarkers and cancer incidence and mortality: is there an association? *Cardiovasc Res*. 2021;118:2317–2328. doi: 10.1093/cvr/cvab282

13. Koelwyn GJ, Aboumsallem JP, Moore KJ, de Boer RA. Reverse cardio-oncology: exploring the effects of cardiovascular disease on cancer pathogenesis. *J Mol Cell Cardiol*. 2022;163:1–8. doi: 10.1016/j.yjmcc.2021.09.008

14. Mathieu M, Martin-Jaular L, Lavieu G, Thery C. Specificities of secretion and uptake of exosomes and other extracellular vesicles for cell-to-cell communication. *Nat Cell Biol*. 2019;21:9–17. doi: 10.1038/s41556-018-0250-9

15. Sahoo S, Adamiak M, Mathiyalagan P, Kenneweg F, Kafert-Kasting S, Thum T. Therapeutic and diagnostic translation of extracellular vesicles in cardiovascular diseases: roadmap to the clinic. *Circulation*. 2021;143:1426–1449. doi: 10.1161/CIRCULATIONAHA.120.049254

16. Lucotti S, Kenific CM, Zhang H, Lyden D. Extracellular vesicles and particles impact the systemic landscape of cancer. *EMBO J*. 2022;41:e109288. doi: 10.15252/embj.2021109288

17. Kalluri R, McAndrews KM. The role of extracellular vesicles in cancer. *Cell*. 2023;186:1610–1626. doi: 10.1016/j.cell.2023.03.010

18. Gabisonia K, Khan M, Recchia FA. Extracellular vesicle-mediated bidirectional communication between heart and other organs. *Am J Physiol Heart Circ Physiol*. 2022;322:H769–H784. doi: 10.1152/ajpheart.00659.2021

19. Moliner P, Lupon J, de Antonio M, Domingo M, Santiago-Vacas E, Zamora E, Cediel G, Santesmases J, Diez-Quevedo C, Troya MI, et al. Trends in modes of death in heart failure over the last two decades: less sudden death but cancer deaths on the rise. *Eur J Heart Fail*. 2019;21:1259–1266. doi: 10.1002/ejhf.1569

20. Loyer X, Zlatanova I, Devue C, Yin M, Howangyin KY, Klaihmon P, Guerin CL, Kheloufi M, Vilar J, Zannis K, et al. Intra-cardiac release of extracellular vesicles shapes inflammation following myocardial infarction. *Circ Res*. 2018;123:100–106. doi: 10.1161/CIRCRESAHA.117.311326

21. Shaihov-Teper O, Ram E, Ballan N, Brzezinski RY, Naftali-Shani N, Masoud R, Ziv T, Lewis N, Schary Y, Levin-Kotler LP, et al. Extracellular vesicles from epicardial fat facilitate atrial fibrillation. *Circulation*. 2021;143:2475–2493. doi: 10.1161/CIRCULATIONAHA.120.052009

22. Thery C, Witwer KW, Aikawa E, Alcaraz MJ, Anderson JD, Andriantsitohaina R, Antoniou A, Arab T, Archer F, Atkin-Smith GK, et al. Minimal information for studies of extracellular vesicles 2018 (MISEV2018): a position statement of the International Society for Extracellular Vesicles and update of the MISEV2014 guidelines. *J Extracell Vesicles*. 2018;7:1535750. doi: 10.1080/20013078.2018.1535750

23. Tucker NR, Chaffin M, Fleming SJ, Hall AW, Parsons VA, Bedi KC Jr., Akkad AD, Herndon CN, Arduini I, Papangeli I, et al. Transcriptional and cellular diversity of the human heart. *Circulation*. 2020;142:466–482. doi: 10.1161/CIRCULATIONAHA.119.045401

24. Litvinukova M, Talavera-Lopez C, Maatz H, Reichart D, Worth CL, Lindberg EL, Kanda M, Polanski K, Heinig M, Lee M, et al. Cells of the adult human heart. *Nature*. 2020;588:466–472. doi: 10.1038/s41586-020-2797-4

25. Dominici M, Le Blanc K, Mueller I, Slaper-Cortenbach I, Marini F, Krause D, Deans R, Keating A, Prockop D, Horwitz E. Minimal criteria for defining multipotent mesenchymal stromal cells. The International Society for Cellular Therapy position statement. *Cytotherapy*. 2006;8:315–317. doi: 10.1080/14653240600855905

26. Naftali-Shani N, Levin-Kotler LP, Palevski D, Amit U, Kain D, Landa N, Hochhauser E, Leor J. Left ventricular dysfunction switches mesenchymal stromal cells toward an inflammatory phenotype and impairs their reparative properties via Toll-like receptor-4. *Circulation*. 2017;135:2271–2287. doi: 10.1161/CIRCULATIONAHA.116.023527

27. Koliaraki V, Prados A, Armaka M, Kollias G. The mesenchymal context in inflammation, immunity and cancer. *Nat Immunol*. 2020;21:974–982. doi: 10.1038/s41590-020-0741-2

28. Carlson S, Trial J, Soeller C, Entman ML. Cardiac mesenchymal stem cells contribute to scar formation after myocardial infarction. *Cardiovasc Res*. 2011;91:99–107. doi: 10.1093/cvr/cvr061

29. Galland S, Stamenkovic I. Mesenchymal stromal cells in cancer: a review of their immunomodulatory functions and dual effects on tumor progression. *J Pathol*. 2020;250:555–572. doi: 10.1002/path.5357

30. Daseke MJ 2nd, Tenkorang MAA, Chalise U, Konfrst SR, Lindsey ML. Cardiac fibroblast activation during myocardial infarction wound healing: fibroblast polarization after MI. *Matrix Biol*. 2020;91-92:109–116. doi: 10.1016/j.matbio.2020.03.010

31. Tallquist MD, Molkentin JD. Redefining the identity of cardiac fibroblasts. *Nat Rev Cardiol*. 2017;14:484–491. doi: 10.1038/nrcardio.2017.57

32. Pathan M, Fonseka P, Chitti SV, Kang T, Sanwlani R, Van Deun J, Hendrix A, Mathivanan S. Vesiclepedia 2019: a compendium of RNA, proteins, lipids and metabolites in extracellular vesicles. *Nucleic Acids Res*. 2019;47:D516–D519. doi: 10.1093/nar/gky1029

33. Hanahan D. Hallmarks of cancer: new dimensions. *Cancer Discov*. 2022;12:31–46. doi: 10.1158/2159-8290.CD-21-1059

34. Fitzgerald W, Freeman ML, Lederman MM, Vasilieva E, Romero R, Margolis L. A system of cytokines encapsulated in extracellular vesicles. *Sci Rep*. 2018;8:8973. doi: 10.1038/s41598-018-27190-x

35. Barnes BJ, Somerville CC. Modulating cytokine production via select packaging and secretion from extracellular vesicles. *Front Immunol*. 2020;11:1040. doi: 10.3389/fimmu.2020.01040

36. Narayan V, Thompson EW, Demissei B, Ho JE, Januzzi JL, Ky B. Mechanistic biomarkers informative of both cancer and cardiovascular disease: JACC state-of-the-art review. *J Am Coll Cardiol*. 2020;75:2726–2737. doi: 10.1016/j.jacc.2020.03.067

37. Mantovani A, Allavena P, Marchesi F, Garlanda C. Macrophages as tools and targets in cancer therapy. *Nat Rev Drug Discov*. 2022;21:799–820. doi: 10.1038/s41573-022-00520-5

38. Derynck R, Turley SJ, Akhurst RJ. TGFβ biology in cancer progression and immunotherapy. *Nat Rev Clin Oncol*. 2021;18:9–34. doi: 10.1038/s41571-020-0403-1

39. Riffo-Campos AL, Riquelme I, Brebi-Mieville P. Tools for sequence-based miRNA target prediction: what to choose? *Int J Mol Sci*. 2016;17:1987. doi: 10.3390/ijms17121987

40. Pollard JW. Tumour-educated macrophages promote tumour progression and metastasis. *Nat Rev Cancer*. 2004;4:71–78. doi: 10.1038/nrc1256

41. Rotem I, Konfino T, Caller T, Schary Y, Shaihov-Teper O, Palevski D, Lewis N, Lendengolts D, Naftali-Shani N, Leor J. Osteopontin promotes infarct repair. *Basic Res Cardiol*. 2022;117:51. doi: 10.1007/s00395-022-00957-0

42. Zhang H, Liu L, Liu J, Dang P, Hu S, Yuan W, Sun Z, Liu Y, Wang C. Roles of tumor-associated macrophages in anti-PD-1/PD-L1 immunotherapy for solid cancers. *Mol Cancer*. 2023;22:58. doi: 10.1186/s12943-023-01725-x

43. Catalano M, O'Driscoll L. Inhibiting extracellular vesicles formation and release: a review of EV inhibitors. *J Extracell Vesicles*. 2020;9:1703244. doi: 10.1080/20013078.2019.1703244

44. Motiei M, Dreifuss T, Betzer O, Panet H, Popovtzer A, Santana J, Abourbeh G, Mishani E, Popovtzer R. Differentiating between cancer and inflammation: a metabolic-based method for functional computed tomography imaging. *ACS Nano*. 2016;10:3469–3477. doi: 10.1021/acsnano.5b07576

45. Pitt B, Zannad F, Remme WJ, Cody R, Castaigne A, Perez A, Palensky J, Wittes J. The effect of spironolactone on morbidity and mortality in patients with severe heart failure. Randomized Aldactone Evaluation Study Investigators. *N Engl J Med*. 1999;341:709–717. doi: 10.1056/NEJM199909023411001

46. Ferreira JP, Verdonschot J, Wang P, Pizard A, Collier T, Ahmed FZ, Brunner-La-Rocca H-P, Clark AL, Cosmi F, Cuthbert J, et al; HOMAGE (Heart Omics in AGEing) Consortium. Proteomic and mechanistic analysis of spironolactone in patients at risk for HF. *JACC Heart Fail*. 2021;9:268–277. doi: 10.1016/j.jchf.2020.11.010

47. Shi C, Aboumsallem JP, de Wit S, Schouten EM, Bracun V, Meijers WC, Silljé HHW, de Boer RA. Evaluation of renal cancer progression in a mouse model of heart failure. *Cancer Commun (Lond)*. 2021;41:796–799. doi: 10.1002/cac2.12185

48. Yuan Y, Mei Z, Qu Z, Li G, Yu S, Liu Y, Liu K, Shen Z, Pu J, Wang Y, et al. Exosomes secreted from cardiomyocytes suppress the sensitivity of tumor ferroptosis in ischemic heart failure. *Signal Transduct Target Ther*. 2023;8:121. doi: 10.1038/s41392-023-01336-4

49. Oh AR, Park J, Lee J-H, Min JJ, Gook J, Jang JN, Lee S-H, Kim K, Ahn J. The use of renin angiotensin aldosterone system inhibitors may be associated with decreased mortality after cancer surgery. *Sci Rep*. 2022;12:6838. doi: 10.1038/s41598-022-10759-y

50. Naftali-Shani N, Itzhaki-Alfia A, Landa-Rouben N, Kain D, Holbova R, Adutler-Lieber S, Molotski N, Asher E, Grupper A, Millet E, et al. The origin of human mesenchymal stromal cells dictates their reparative properties. *J Am Heart Assoc*. 2013;2:e000253. doi: 10.1161/JAHA.113.000253

51. Zacchigna S, Paldino A, Falcao-Pires I, Daskalopoulos EP, Dal Ferro M, Vodret S, Lesizza P, Cannata A, Miranda-Silva D, Lourenco AP, et al. Towards standardization of echocardiography for the evaluation of left ventricular function in adult rodents: a position paper of the ESC Working Group on Myocardial Function. *Cardiovasc Res*. 2021;117:43–59. doi: 10.1093/cvr/cvaa110

52. Leroyer AS, Ebrahimian TG, Cochain C, Recalde A, Blanc-Brude O, Mees B, Vilar J, Tedgui A, Levy BI, Chimini G, et al. Microparticles from ischemic muscle promotes postnatal vasculogenesis. *Circulation*. 2009;119:2808–2817. doi: 10.1161/CIRCULATIONAHA.108.816710

53. Deutsch EW, Bandeira N, Sharma V, Perez-Riverol Y, Carver JJ, Kundu DJ, Garcia-Seisdedos D, Jarnuczak AF, Hewapathirana S, Pullman BS, et al. The ProteomeXchange consortium in 2020: enabling "big data" approaches in proteomics. *Nucleic Acids Res*. 2020;48:D1145–D1152. doi: 10.1093/nar/gkz984

54. Perez-Riverol Y, Bai J, Bandla C, Garcia-Seisdedos D, Hewapathirana S, Kamatchinathan S, Kundu DJ, Prakash A, Frericks-Zipper A, Eisenacher M, et al. THE PRIDE database resources in 2022: a hub for mass spectrometry-based proteomics evidences. *Nucleic Acids Res*. 2022;50:D543–D552. doi: 10.1093/nar/gkab1038

55. Kozomara A, Birgaoanu M, Griffiths-Jones S. miRBase: from microRNA sequences to function. *Nucleic Acids Res*. 2019;47:D155–D162. doi: 10.1093/nar/gky1141

56. Hosen MR, Goody PR, Zietzer A, Xiang X, Niepmann ST, Sedaghat A, Tiyerili V, Chennupati R, Moore JB, Boon RA, et al. Circulating microRNA-122-5p is associated with a lack of improvement in left ventricular function after transcatheter aortic valve replacement and regulates viability of cardiomyocytes through extracellular vesicles. *Circulation*. 2022;146:1836–1854. doi: 10.1161/CIRCULATIONAHA.122.060258

57. Schneider CA, Rasband WS, Eliceiri KW. NIH Image to ImageJ: 25 years of image analysis. *Nat Methods*. 2012;9:671–675. doi: 10.1038/nmeth.2089

58. Kuang Tzu Huang YHC, Walker AM. Inaccuracies in MTS assays: major distorting effects of medium, serum albumin, and fatty acids. *Biotechniques*. 2004;37:406–412. doi: 10.2144/04373ST05

59. Wang Y, Alexander JS. Analysis of endothelial barrier function in vitro. *Methods Mol Biol*. 2011;763:253–264. doi: 10.1007/978-1-61779-191-8_17

60. Lallemand T, Rouahi M, Swiader A, Grazide MH, Geoffre N, Alayrac P, Recazens E, Coste A, Salvayre R, Negre-Salvayre A, et al. nSMase2 (type 2-neutral sphingomyelinase) deficiency or inhibition by GW4869 reduces inflammation and atherosclerosis in Apoe⁻/⁻ mice. *Arterioscler Thromb Vasc Biol*. 2018;38:1479–1492. doi: 10.1161/ATVBAHA.118.311208

61. Dinkins MB, Dasgupta S, Wang G, Zhu G, Bieberich E. Exosome reduction in vivo is associated with lower amyloid plaque load in the 5XFAD mouse model of Alzheimer's disease. *Neurobiol Aging*. 2014;35:1792–1800. doi: 10.1016/j.neurobiolaging.2014.02.012